Geoscience Frontiers xxx (2018) 1–27

HOSTED BY

ELSEVIER

Contents lists available at ScienceDirect

China University of Geosciences (Beijing)

Geoscience Frontiers

journal homepage: www.elsevier.com/locate/gsf

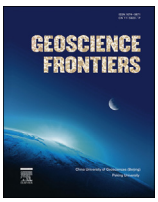

Research Paper

The significance of U–Pb zircon ages in zoned plutons– the case of the Flamenco pluton, Coastal Range batholith, northern Chile

Natalia Rodríguez [a], Juan Díaz-Alvarado [a,*], Carlos Fernández [b], Paulina Fuentes [a], Christoph Breitkreuz [c], Colombo Celso Gaeta Tassinari [d]

[a] Departamento de Geología, Universidad de Atacama, Copayapu 485, Copiapó, Chile
[b] Departamento de Ciencias de la Tierra, Universidad de Huelva, E-21071, Huelva, Spain
[c] Institut für Geologie, TU Bergakademie Freiberg, Bernhard von Cotta Str. 2, 09599, Freiberg, Germany
[d] High Resolution Geochronological Laboratory University of São Paulo, Rua do lago 562, São Paulo, SP, Brazil

ARTICLE INFO

Article history:
Received 30 October 2017
Received in revised form
29 April 2018
Accepted 10 June 2018
Available online xxx
Handling Editor: Christopher J Spencer

Keywords:
Zircon U–Pb geochronology
Zoned plutons
Andean magmatic arc
Sequential emplacement
Individual and statistical zircon ages

ABSTRACT

Compositionally zoned plutons, both layered and concentrically arranged, provide granitic exposures where the mechanisms and timing of the magmatic emplacement processes can be studied. The importance of in-situ geochemical differentiation and the magma replenishment rates are revealed by geochemistry and field relations, together with the increasingly accurate U–Pb geochronology, which has promoted the knowledge about the pluton incremental assembly theories.

The Flamenco pluton, located in the Coastal Range of northern Chile, is part of the Upper Triassic to Early Cretaceous Andean intrusives formed in the western active margin of South America, and present a normal zoned structure with mafic magmatic facies (mostly gabbros and Qtz-diorites) close to the contacts with the host metasediments, and tonalites, granodiorites and granites in the inner areas. A combined study of the field relations, geochemistry and zircon geochronology of the magmatic facies was applied to determine the emplacement sequence of the Flamenco pluton, revealing three distinguishable domains separated by metasedimentary septa. The SW area is constituted by mostly homogeneous leucocratic granodiorites that yielded an age of 213 Ma as the best estimation for their emplacement age. Distinctive geochemical characteristics, such as the absence of an Eu anomaly, the depletion in HREE, or the highest Sr, Sr/Y and Ce/Yb values among the granodioritic facies of the pluton, involve lower T and/or higher P conditions at the magmatic source according to experimental studies. These conditions were established during an early stage of the Andean magmatic arc building that is firstly defined here as Upper Triassic. The NW and E domains of the pluton were sequentially emplaced between 194 Ma and 186 Ma and both the field relations and the detailed geochronological results suggest that the mafic facies intruded latter in the emplacement sequence. To the NW, Qtz-dioritic and gabbroic externally emplaced pulses gave a younger crystallization age of 186.3 ± 1.8 Ma, and promoted the granoblastic textures and metamorphic zircon overgrowths that characterize the granodiorites located in the contact with the intermediate and felsic inner magmas, which yielded a best estimation of their emplacement age of 192 ± 1.5 Ma. On the other hand, in the eastern domain, magma-magma relations are observed between gabbros and previously intruded tonalites and granodiorites. Both the mafic and intermediate facies show two main subgroups of ages that yielded 194.7 ± 1.5 Ma to 188.3 ± 2.1 Ma and 193.1 ± 2.2 Ma to 185.5 ± 1.4 Ma respectively. These differences are related to the variations in the magmatic addition rates, which may extend the super-solidus conditions in the eastern domain of the magmatic reservoir as is confirmed by the wider age ranges yielded by these magmatic facies. Zircon overgrowths in the host rocks yield similar ages (around 220 Ma and 205 Ma) than the oldest results obtained in the intrusive facies, indicating that metamorphism correlates with the initial stages of plutonic emplacement.

Geochronological results differ between 9 Myr and 41 Myr in the eight studied samples for non-inherited ages and gave very close mean ages (within analytical uncertainty) for all the intrusive units. However, we examine other characteristics such as zircon morphology, internal structure,

* Corresponding author.
E-mail address: juan.diaza@uda.cl (J. Díaz-Alvarado).
Peer-review under responsibility of China University of Geosciences (Beijing).

https://doi.org/10.1016/j.gsf.2018.06.003

geochemistry and statistical data to assess if the scattering of the geochronological data may be related to the different processes involved in the construction of the Flamenco pluton. We concluded that this detailed study of U–Pb zircon ages, including individual and significative groups of analyses, is useful to determine accurately the emplacement sequence and the genetic relation between the intrusive units, together with the evidences depicted by the geochemistry and field relations.

1. Introduction

Magmatic arcs established in active continental margins are the crustal setting where the most voluminous and diverse igneous rock relations are recognized (Wyllie, 1977; Hawkesworth and Kemp, 2006; Castro, 2013). In addition, the rate of development and the geochemical evolution of these continental arcs provide key pieces of evidence in the study of continental margins (e.g. Rudnick, 1995; Hawkesworth and Kemp, 2006; DeCelles et al., 2009; Ducea et al., 2015a, b). As paradigmatic examples, portions of the Andean, Famatinian and Pampean continental arcs are preserved in western South America (e.g Rapela et al., 1990; Parada et al., 2007; Otamendi et al., 2009; Castro et al., 2011, 2014). Based on their spatial, temporal and geochemical relations, subduction is suggested to be the main engine for arc magmatism and the formation of large Cordilleran-type batholiths (e.g. Wyllie et al., 1976; Wyllie, 1977; Castro et al., 2010).

The geochemistry of arc magmatism is characterized by the compositional homogeneity at the large scale and the mantle/crust hybrid isotopic signatures (e.g. Pankhurst et al., 1999; Burgisser and Bergantz, 2011; Castro, 2013). Studies focused on geochemical characteristics of arc magmatism, such as the Sr/Y ratios and the rare earth elements (REE) patterns and their relation with the crustal thickness (e.g. Chapman et al., 2015; Ducea et al., 2015a), do not often delve into the phase relations and the T-P-XH_2O conditions during the generation of Cordilleran-type magmatism, and most studies only consider a MASH zone (melting, assimilation, storage, homogenization) (Hildreth and Moorbath, 1988) in the arc root as the source area where the compositional diversity of arc magmatism is though to originate (Chapman et al., 2015; Walker et al., 2015). However, a large number of experimental works (Sisson et al., 2005; Alonso Perez et al., 2009; Castro et al., 2010) and numerical models (e.g. Annen et al., 2006; Gerya and Stoeckhert, 2006; Gorczyk et al., 2007) show the complexity of the genesis of the intermedium- to high-silica magmatism (e.g. Castro, 2013; Frost et al., 2016), and mid- to lower-crustal (e.g. De Paolo, 1981; Patiño-Douce, 1995; Thompson et al., 2002; Annen et al., 2006; Clemens et al., 2011) and lithospheric mantle ("off-crust") (Castro and Gerya, 2008; Castro et al., 2010; Chen and Zhao, 2017) scenarios have been suggested as appropriate petrogenetic conditions and source areas. Further, zircon geochemistry (including isotopic signatures) has been integrated into petrogenetic studies because it is a fairly good recorder of temperature, pressure and melt compositions that prevail during zircon growth (e.g. Watson and Harrison, 1983; Miller et al., 2003; Teixeira et al., 2011; Jeon et al., 2012; Villaseca et al., 2012). Regardless of the model proposed for the origin of the arc magmatism, the cyclicity in the magmatic addition rates and the geochemical signatures during the evolution of Cordilleran orogenic systems must be taken into account to study the processes involved in the genesis and emplacement of this magmatism (e.g. DeCelles et al., 2009; Chiaradia, 2015; Ducea et al., 2015b; Paterson and Ducea, 2015; Cao et al., 2016; Kirsch et al., 2016).

The determination of relevant parameters of plutonic bodies such as the shape, dimensions, volume, composition and timing of emplacement and crystallization adds important constraints to the geochemical and rheological evolution of magmas and their relation to tectonic events (e.g. Hecht and Vigneresse, 1999; Bachmann and Huber, 2016). Field relations, geophysical, gravity and magnetic data provide key constraints on the nature of pluton contacts and structures associated with pluton margins (e.g. Bouchez, 1997; Hecht and Vigneresse, 1999). Detailed geochemical and field studies are used to establish the zonation of magmatic facies and to determine the pristine geochemical characteristics vs. those acquired during the emplacement process (e.g. assimilation, contamination, mingling, among others) (Díaz-Alvarado et al., 2011; Clemens and Stevens, 2012; Fiannacca et al., 2015; Díaz-Alvarado, 2017).

The building and the final structure of zoned plutons, including both layered and concentrically arranged granitic bodies, are determined by the relation between the emplacement rate and the deformation of the crust (tectonic or magma-related) (e.g. Vigneresse, 1995; Hecht et al., 1997; Annen et al., 2006; Díaz-Alvarado et al., 2012). Low magma supply induces the outer emplacement of the latter magma batches due to the rigid state of the almost crystallized previously intruded magmas. With higher emplacement rates, latter magma pulses may develop enough force to overcome the strength of the partially melted earlier magma batches promoting melt percolation through the constituted crystal mush and the interaction between early and late magmatic batches (Vigneresse et al., 1996; Hecht and Vigneresse, 1999; Bachmann and Bergantz, 2004, 2008; Miller et al., 2011).

It should be noted that the current understanding of the building of batholiths by sequential emplacement or magmatic pulse assembly models (Coleman et al., 2004; Glazner et al., 2004) was triggered by the progress in the U–Pb zircon geochemistry and geochronology (Watson and Harrison, 1983; Williams, 1998; Miller et al., 2003, 2007, 2011). The wide range of ages (1–10 Myr for many plutons in convergent settings, e.g. de Saint Blanquat et al., 2011) obtained for large composite batholiths using U–Pb zircon geochronology have been tested by numerical models that determine the rheological and thermal conditions in which the addition and preservation of silicic magma reservoirs are produced (e.g. Bachmann et al., 2002; Paterson et al., 2008, 2011; Huber et al., 2011; Díaz-Alvarado et al., 2013). Zircon ages from plutonic rocks provide constraints on remobilization, rejuvenation or long-standing crystal-rich mushes, with implications for the plutonic-volcanic association (e.g. Bachmann and Bergantz, 2004; Huber et al., 2010; Huber et al., 2011; Bachmann and Huber, 2016). However, geochronological results that commonly suggest the long-lasting supersolidus evolution of crustal magmatic reservoirs are inconsistent with other evidences, such as the crystal size distributions and elemental diffusion modeling (e.g. Pappalardo and Mastrolorenzo, 2012; Cooper and Kent, 2014), which may actually reflect other processes or underestimate the timescales obtained from the U–Pb geochronology (Bachmann and Huber, 2016).

Modern U–Pb zircon geochronology has expanded the methodological scope to solve a wide diversity of geological problems. Mean zircon ages are useful to obtain approximate crystallization ages of plutons in vast batholithic areas (e.g. Castro et al., 2011).

Please cite this article in press as: Rodríguez, N., et al., The significance of U–Pb zircon ages in zoned plutons– the case of the Flamenco pluton, Coastal Range batholith, northern Chile, Geoscience Frontiers (2018), https://doi.org/10.1016/j.gsf.2018.06.003

Individual or cluster of ages determinated in single magmatic facies have been examined in order to constrain the timescales and evolution of batholith construction in different tectonic environments (e.g. Miller et al., 2007; de Saint Blanquat et al., 2011; Díaz-Alvarado et al., 2013; Paterson and Ducea, 2015; Fiannacca et al., 2017). Besides, in order to date the eruptive processes, youngest U–Pb zircon ages are usually considered in effusive rocks (e.g. Chamberlain et al., 2014), although co-genetic older zircons (antecrysts) may yield the age of the pre-eruptive evolution of the magma chamber (e.g. Bachmann and Huber, 2016; Aragón et al., 2017). Metamorphic zircon overgrowths and detrital zircons are also significant when dating metamorphic and sedimentary terranes (e.g. Wang et al., 2011; Pereira et al., 2012).

Age determinations, as emplacement ages, are interpreted from large time gaps, up to several million years, found in U–Pb zircon geochronological data, i.e. concordia and weighted mean ages, estimated crystallization ages based on age clusters and individual ages, and the significance of geochronological results in the context of pluton construction often remain unclear. We present here a combined study of the contact relations, geochemistry and zircon geochronology of the different magmatic facies that comprise the zoned Flamenco pluton in northern Chile to constrain the emplacement sequence of the pluton and prompt a thorough discussion around the significance of individual and statistical data in geochronology. Besides, this work provides new geochronological and geochemical results about the earliest stages of the magmatic arc construction during the beginning of the Andean cycle.

2. Geological setting

In the central segment of the western margin of South America, the Paleozoic was characterized by the accretion of terranes to the subductive margin (e.g. Mpodozis and Ramos, 1989). The pre-Andean cycle, after the assembly of the Gondwana megacontinent and prior to its break-up, comprised a series of tectonic events that culminated in the Lower Jurassic with the westward shift of the magmatic arc to the present Chilean coast (e.g. Mpodozis and Ramos, 1989; Charrier et al., 2007). This major tectonic change coincided with the deposition of continental sequences and andesitic and dacitic volcanosedimentary rocks to the east (La Ternera Formation: e.g. Suárez and Bell, 1992; Iriarte et al., 1999) and the beginning of the Andean cycle. The First Stage (Charrier et al., 2007) of the Andean cycle in northern Chile was characterized by a magmatic arc parallel to the western margin of Gondwana, with a back-arc basin on its eastern side comprised by interconnected basins, between the Lower Jurassic and the late Lower Cretaceous. The location of the magmatic arc in these stages is well documented by the Jurassic volcanic rocks included in the La Negra Formation, and the plutons that comprise the Coastal Range batholith (Suárez et al., 1985; Dallmeyer et al., 1996; Scheuber and González, 1999). Jurassic plutonic rocks are mainly calc-alkaline tonalites and granodiorites, with minor amounts of gabbros, Qtz-diorites and granites, with abundant mafic enclaves and synplutonic dikes. The wide silica content variation characterizes a medium- to high-K calc-alkaline series with similar trace elements geochemical signatures as moderate $(La/Yb)_N$ values and negative Eu anomalies (e.g. Parada, 1992; Dallmeyer et al., 1996; Parada et al., 1999). The range of pressures estimated for the emplacement crustal levels of the batholiths to the south of the study area is comprised between 3 and 5 kbars (Gana and Tosdal, 1996). Among the oldest Mesozoic Cordilleran-type intrusives described in the Coastal Range batholith in northern Chile are the Carrizal Bajo Plutonic complex that yields an age range between 208 Ma and 206 Ma and the Algodones Granite of 203–199 Ma (Welkner et al., 2006; Arévalo and Welkner, 2008; Creixell et al., 2012).

From the Lower Jurassic to the Lower Cretaceous, the arc axis was displaced around 50 km to the east (Fig. 1a,b). The geological record strongly supports the long-lasting magmatic addition during this period, generated during an extensional regime and crustal thinning (Parada et al., 2007). Plutonic complexes are interrupted by the Atacama Fault System (AFS) (Fig. 1b), whose main activity is evidenced by the elongated shape and the ductile deformation and mylonites observed in the Upper Jurassic plutons (Brown et al., 1993; Grocott and Taylor, 2002). This roughly N–S to NW–SE fault system extends for more than 1000 km between Iquique (21°S) and La Serena (30°S) and is characterized by mainly sinistral strike-slip movements, as well as vertical displacements in its first stages (Arabasz, 1971). The AFS has been related to the oblique (NW–SE) convergence of the Aluk (Phoenix) plate relative to the South American continent (e.g. Scheuber et al., 1994). The Lower Cretaceous plutons were emplaced to the east of the principal fault (Fig. 1b).

The Flamenco pluton is part of an N–S alignment of the Upper Triassic to Lower Jurassic intrusive belt comprising the westernmost part of the Coastal Range batholith in northern Chile. It is mainly composed of Cpx-Hbl-Bt granodiorites and tonalites towards the contacts with the metasedimentary host-rocks (mineral abbreviations by Kretz, 1983). Monzodiorites, Qtz-diorites and gabbros are present in lower proportion (Godoy and Lara, 1998). Together, the intrusives form a calcic, magnesian and metaluminous magmatic series, typical of syn-collisional volcanic arc settings. A protracted emplacement process has been proposed for the Flamenco pluton according to the field relations and the granulitization textures observed in some intrusive units, acquired during the successive intrusion of magmatic pulses (Rodríguez et al., 2016). The Flamenco pluton is intruded by conjugate sets of andesitic NE–SW and subordinate NW–SE dikes (Dallmeyer et al., 1996). A more accurate description of the geochemical and geochronological characteristics of the pluton and the emplacement process is presented in this study.

Between 29°S and 26°S in northern Chile, Jurassic magmatism was emplaced in the metasedimentary Las Tórtolas Formation. This formation has been interpreted as a late Paleozoic accretionary prism formed by a sequence of interbedded sandstones and shales, with minor limestones, pelagic chert and conglomerates, and tectonically deformed and metamorphosed to greenschist facies (Bell, 1982, 1987; Fuentes et al., 2016). Recently, the Las Tórtolas Formation has been divided into three petrologically and structurally distinguishable domains that are, from west to east: the mélange facies, characterized by an intense ductile deformation and a block-in-matrix texture; the volcanic domain, mainly comprised by N- and E-MORB basaltic rocks, with minor tuffs and rhyolites; and the Eastern Series defined by the thrust faults and associated fault-propagation folds that affected the turbiditic succession (Fuentes et al., 2017). This approximately N–S structural and petrological zonation of the metasedimentary basement is cross-cut by the Flamenco pluton contacts.

3. Intrusive units description and field relations

The Flamenco pluton, located to the west of the Coastal Range batholith in northern Chile (Fig. 1a,b), shows an almost continuous granitic exposure covering a surface of around 350–400 km^2 (Fig. 1c,d). The Flamenco pluton outcrops are divided into three areas that are in contact with metasedimentary septa that pertain to the Las Tórtolas Formation. To the SW, the granitic facies consist of mostly homogeneous leucocratic granodiorites. To the east, these granodiorites are in contact with the metasedimentary host-rocks along a sharp contact zone dipping between 70° and 85° to the east (Fig. 2a). To the north, they are in contact with the NW area

Please cite this article in press as: Rodríguez, N., et al., The significance of U–Pb zircon ages in zoned plutons– the case of the Flamenco pluton, Coastal Range batholith, northern Chile, Geoscience Frontiers (2018), https://doi.org/10.1016/j.gsf.2018.06.003

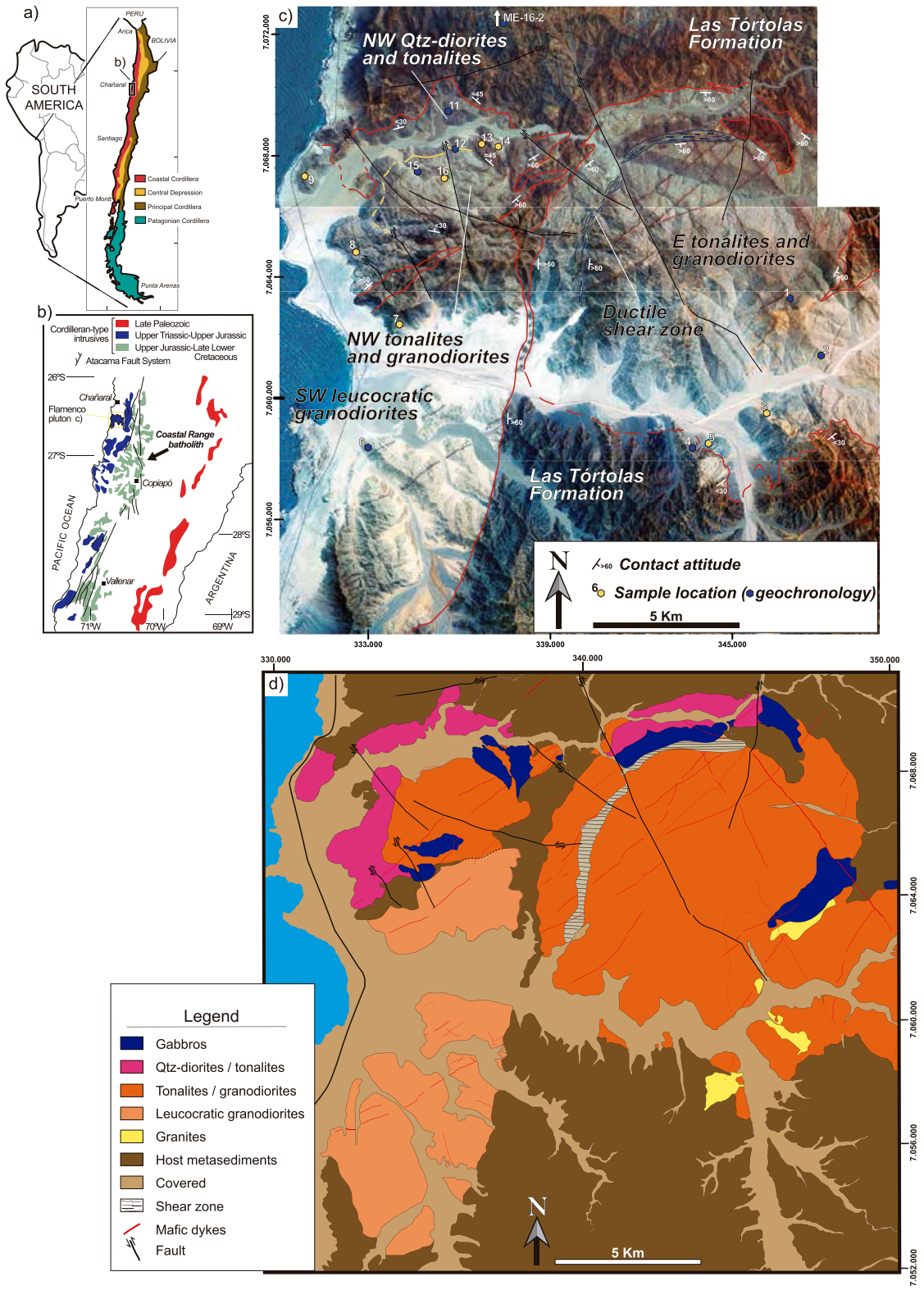

Figure 1. (a) Major morphological features of the Andean cordillera in Chile (modified from Charrier et al., 2007). (b) Sketch of a section of the west margin of Southamerica from 29°S to 26°S showing the distribution of the Cordilleran-type magmatism between the late Paleozoic to the late Lower Cretaceous (Coastal Range batholith) (modified from Charrier et al., 2007; Maksaev et al., 2014). Major faults that comprise the Atacama Fault System are indicated. (c) Satellite image of the Flamenco pluton. The contacts with the host metasediments (red lines), the main intrusive units and some structural features are pointed over the image. The locations of the samples employed in the geochemical and geochronological study are indicated. (d) Geological map of the Flamenco pluton with the main mesoscopic petrological units.

Please cite this article in press as: Rodríguez, N., et al., The significance of U–Pb zircon ages in zoned plutons– the case of the Flamenco pluton, Coastal Range batholith, northern Chile, Geoscience Frontiers (2018), https://doi.org/10.1016/j.gsf.2018.06.003

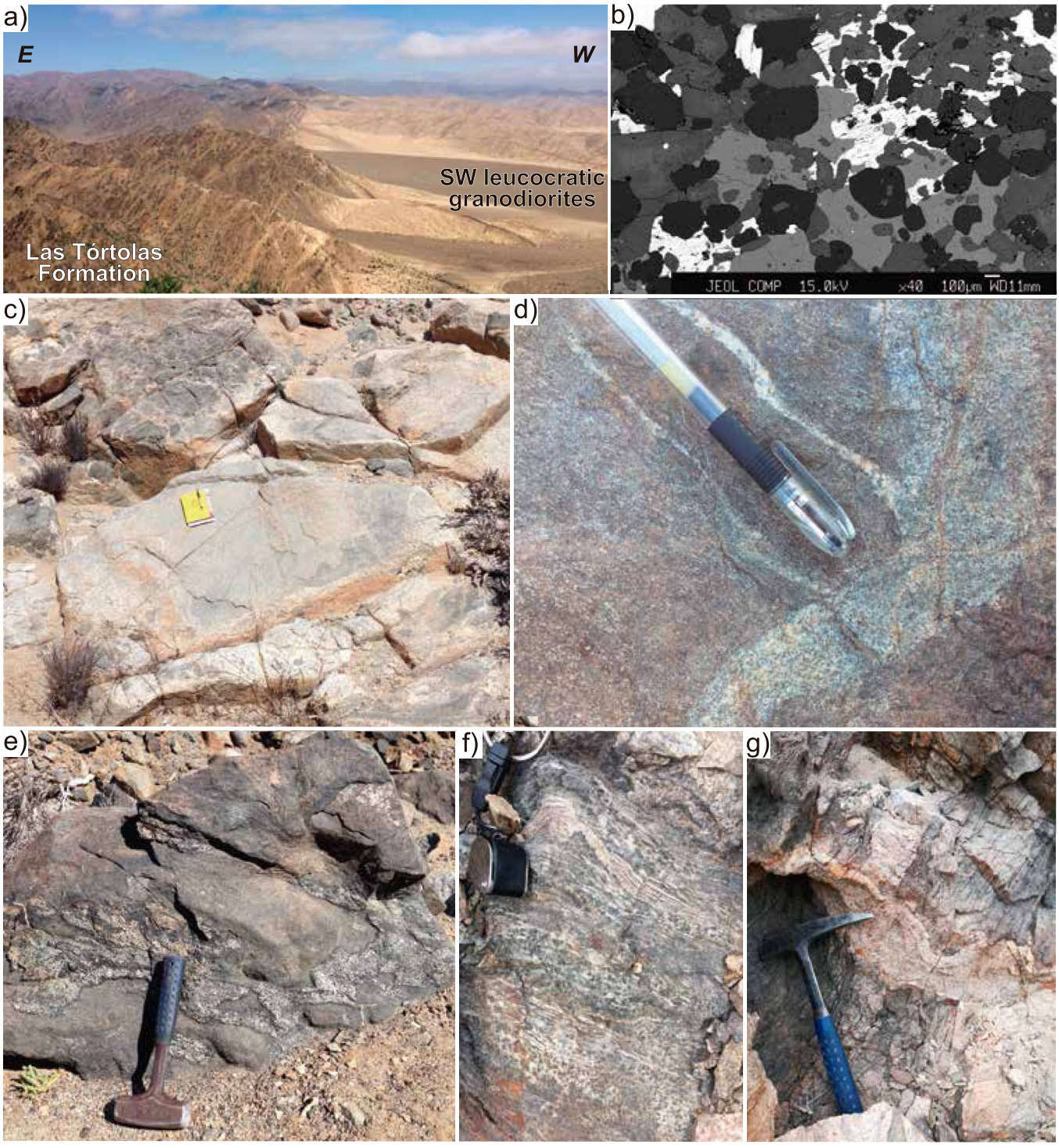

Figure 2. (a) View (to the south) of the southern contact of the Flamenco pluton where the Las Tórtolas Formation are located above the SW leucocratic granodiorites. (b) Mesocratic granodiorites located between the NW Qtz-diorites and tonalites and NW tonalites and granodiorites (yellow line in Fig. 1c) present granulitic recrystallization textures. These rocks show Hbl-Pl-Qtz triple junctions and poikiloblastic Kfs. (c) Mingling areas between gabbros and tonalites located close to the shear zone at the eastern area of the Flamenco pluton (Fig. 1c). Where the gabbroic enclaves are affected by the shear zone, subsolidus fabrics (parallel to the pen in the image) are observed in these gabbros (d). (e), (f) and (g) Las Tórtolas Formation volcanic and sedimentary rocks located in the contact metamorphic aureole of the Flamenco pluton. Recrystallized basalts at the northern contact (e) and Crd-schists (f) to the south present the highest metamorphic grade in the host metasedimentary rocks. There, some thick leucocratic veins and melanosomes (g) characterize a narrow migmatitic domain.

Please cite this article in press as: Rodríguez, N., et al., The significance of U–Pb zircon ages in zoned plutons– the case of the Flamenco pluton, Coastal Range batholith, northern Chile, Geoscience Frontiers (2018), https://doi.org/10.1016/j.gsf.2018.06.003

through a NE–SW trending strip of metasedimentary rocks (Fig. 1c,d).

The NW portion of the Flamenco pluton constitutes a more heterogeneous and petrologically variable domain comprising gabbros, Qtz-diorites, tonalites, granodiorites and minor granites. Mesoscopically, these facies can be separated in a Qtz-dioritic to tonalitic external domain and a mostly granodioritic internal domain, comprising a concentrically zoned area of the Flamenco pluton (Fig. 1d). These petrologically distinguishable domains are in contact through small-to medium-grained mesocratic granodioritic rocks that show granoblastic recrystallization (Fig. 2b). These rocks were metamorphosed to granulite facies conditions during successive emplacement of magma batches (Rodríguez et al., 2016). This domain presents several gabbroic 1–2 km long tabular bodies that show sharp contacts with the other intrusive units. These gabbros are preferentially located close to the contacts with the metasedimentary rocks (Fig. 1c,d). To the north, the NW domain presents gently dipping contacts with the host-rocks. This domain is in contact with the eastern area of the Flamenco pluton through a narrow volcanosedimentary strip that dips more that 60° to the east.

The E domain of the pluton mostly comprises tonalites and granodiorites, with minor gabbros, Qtz-diorites and granites. As in the NW area, several gabbroic bodies are located close to the contacts with the host-rocks (Fig. 1d) and interesting field relations are observed between gabbros and tonalites (Fig. 2c,d). The tabular kilometric gabbroic body (Fig. 1c,d) presents a prominent mingling domain (Fig. 2c) where abundant rounded gabbroic centimetric to metric enclaves are included in a tonalitic host. Magma-magma relations are observed between gabbros and tonalites in these areas. However, the gabbroic body is cross-cutt along its major axis by a ductile shear zone that promoted the stretching of mafic minerals. To the north, this shear zone is E–W trending, parallel to the gabbroic body and to the north contact of the intrusive unit. As the gabbros and the shear zone are closer to the N–S central metasedimentary strip, the trend of the intrusive unit and the shear zone shift to a N–S direction (Fig. 1c,d). Where the shear zone affected the mingling domain, gabbroic enclaves show ductile deformation and a subsolidus fabric is developed. This fabric is not observed in the tonalitic and granodioritic veins that cut the gabbroic magmas during the emplacement and mingling processes (Fig. 2d).

A few leucocratic fine-grained granitic layers cross-cut the magmatic facies along the pluton. The host-rocks do not present a highly developed contact aureole around the Flamenco pluton. Indeed, the northern contact only presents a few meters of Crd-schists and the recrystallization of the volcanic rocks comprised in the Las Tórtolas Formation. The increase of the metamorphic grade associated with the magmatic emplacement is better observed in the central N–S host-rock strip, where the basaltic rocks interbedded with the Crd-schist present an intense Pl and Hbl metamorphic recrystallization (Fig. 2e). At the southern contact, a wider large-to medium-grained Crd-schist area (Fig. 2f) and few localities where migmatitic domains can be observed (Fig. 2g) suggest a higher and longer-lasting thermal input in the contact aureole (Grocott and Taylor, 2002; Rodríguez et al., 2016).

4. Methods

4.1. Sampling and geochemistry analytical techniques

The geochemical characterization of the Flamenco pluton has been based on the analysis of 14 representative samples (location in Fig. 1c). Major and trace element compositions were analyzed at Activation Laboratories Ltda. in Ontario, Canada. Approximately 5 kg of fresh rock was collected from each outcrop. Samples were crushed and milled to a fine powder. Major and trace elements were analyzed by X-ray fluorescence (XRF) and inductively coupled plasma mass spectrometry (ICP-MS) respectively. Major elements were analyzed using the PHILIPS PW 2400 Wavelength Dispersive X-ray Fluorescence Spectrometer. The total uncertainty is determined to be ±100% at the detection limit, ±20% at 10 times the detection limit and ±5% at 100 times the detection limit (relative percentages). Trace elements, including rare earth elements (REE), were analyzed with a Perkin Elmer Sciex ELAN 9000 ICP-MS. Samples are fused with Na_2O_2 at 650–700 °C for 30 min in a Zirconium crucible. The fusion cake formed in the crucible during this process is dissolved in purified water and acidified (room temperature digestion) with concentrated nitric and hydrochloric acids. The total uncertainty is determined to be ≤100% at the detection limit, ≤30% at 10 times the detection limit and ≤20% at 100 times the detection limit (relative percentages).

4.2. SHRIMP analytical procedures

The zircon separates for isotope analyses were obtained by processing all the samples collected following standard crushing, disc-milling, magnetic, and heavy liquids separation in the Geochronological Research Center of the University of São Paulo (IGc-CPGeo-USP). Zircons were afterwards hand-picked and selected. These were further mounted (together with the TEMORA standard) in epoxy and polished to obtain quasi-central sections. After Au-coating, the polished mounts were comprehensively examined with a FEI-QUANTA 250 scanning electron microscope equipped with secondary-electron and cathodoluminescence (CL) detectors at IGc-CPGeo-USP; the most common conditions used in CL analysis were as follows: 60 μA of emission current, 15.0 kV of accelerating voltage, 7 μm of beam diameter, 200 μs of acquisition time, and a resolution of 1024 μm × 884 μm. The same mounts were then analyzed by the U–Pb isotopic technique using a SHRIMP-IIe machine at High Resolution Geochronological Laboratory USP, following the analytical procedures presented in Williams (1998) and Sato et al. (2014). Correction for common Pb was made on the basis of the ^{204}Pb measured, and the typical error component for the $^{206}Pb/^{238}U$ ratio is less than 2%; uranium abundance and U/Pb ratios were calibrated against the TEMORA standard. Analytical uncertainties are 1σ precision estimates. All the analyses listed and plotted were those corrected using the measured ^{204}Pb and a common Pb composition appropriate to the age of each spot (Table 2) (Cummings and Richards, 1975). Concordia ages have been calculated with ISOPLOT 3.0 software (Ludwig, 2003). Ages were calculated using the constants recommended by the IUGS Subcommission on Geochronology (Steiger and Jaeger, 1977), with λ errors and MSWD determined using Concord. + Equiv. Error ellipses and bars in Fig. 8 are 2σ.

5. Results

5.1. Geochemical results

The samples of the Flamenco pluton have been classified according to the R1-R2 (De La Roche et al., 1980) (Fig. 3a) and the total alkali vs. silica (TAS) diagrams (Le Bas et al., 1986; Wilson, 1989) (Fig. 3b). These diagrams are used to group the selected samples from the different areas of the pluton into five compositional fields that are used for the forthcoming descriptions: gabbros, Qtz-diorites, tonalites, granodiorites and granites. Together, the Flamenco pluton magmatic facies form a calc-alkaline, calcic, magnesian and metaluminous series according to the granitoid classification diagrams (Frost et al., 2001) with a wide SiO_2 range (47.8–74.3 wt.%) (Table 1, Fig. 3b,c,e). An almost linear trend is described from Qtz-diorites to granites, although some variations

Please cite this article in press as: Rodríguez, N., et al., The significance of U–Pb zircon ages in zoned plutons– the case of the Flamenco pluton, Coastal Range batholith, northern Chile, Geoscience Frontiers (2018), https://doi.org/10.1016/j.gsf.2018.06.003

Table 1
Whole rock geochemistry results (major composition in wt.% and trace composition in ppm).

Rock type	Gabbros		Qtz-diorite	Tonalites			Granodiorites	
Sample	FL-16-1	FL-16-13	FL-16-11	FL-16-5	FL-16-8	FL-16-9	FL-16-2	FL-16-6
SiO_2	47.8	47.98	55.72	58.43	60.08	62.22	67.38	66.77
TiO_2	1.31	0.91	0.75	0.92	0.65	0.74	0.5	0.48
Al_2O_3	22.5	19.82	17.76	17.01	16.96	17.04	15.01	16.55
Fe_2O_3	8.87	3.83	4.04	7.58	7.11	6.54	3.98	4.42
MgO	3.59	6.2	4.32	3.17	2.93	2.58	1.71	1.78
MnO	0.147	0.2	0.16	0.135	0.135	0.123	0.059	0.073
CaO	11.16	10.37	8.26	6.43	6.15	5.94	3.49	4.23
Na_2O	2.9	2.16	2.69	3.22	3.47	3.59	3.16	4.42
K_2O	0.38	0.18	0.71	1.96	1.33	1.4	3.82	1.58
P_2O_5	0.37	0.12	0.1	0.18	0.12	0.11	0.13	0.12
Co_3O_4	<0.005	-	-	<0.005	<0.005	<0.005	<0.005	<0.005
CuO	0.007	-	-	0.013	0.006	0.006	<0.005	<0.005
NiO	0.004	-	-	0.005	<0.003	<0.003	<0.003	0.005
Cr_2O_3	0.01	-	-	0.01	<0.01	<0.01	0.02	0.01
V_2O_5	0.045	-	-	0.036	0.024	0.022	0.015	0.01
LOI	1.59	1.55	1.11	0.98	0.73	0.51	1.2	0.43
Total	100.7	98.86	99.06	100.1	99.68	100.7	100.5	100.9
La	16.6	5.5	9.2	21	15.2	11.6	26.4	16.1
Ce	35.2	11.9	19.4	46.2	39.1	25	59.6	32.6
Pr	4.6	1.6	2.5	6.1	4.9	3.2	8	4.1
Nd	21.7	7.3	12	25.1	24.1	14.4	30.3	15.8
Sm	4.4	1.8	2.8	5	4.5	3.2	5.6	2.9
Eu	1.8	0.9	1	1.4	1.3	1	1.2	0.9
Gd	4.5	2.2	3.4	4.9	4.6	3.6	5.4	2.7
Tb	0.7	0.4	0.6	0.9	0.7	0.9	0.8	0.4
Dy	3.5	2.7	3.6	4.8	4.4	3.9	4.5	2.4
Ho	0.8	0.6	0.9	1.1	1	0.9	1	0.5
Er	2.1	1.8	2.7	3	3	2.7	2.8	1.5
Tm	0.3	0.2	0.4	0.4	0.4	0.4	0.4	0.2
Yb	1.4	1.8	2.3	3	2.8	2.7	2.5	1.3
Lu	0.27	-	-	0.51	0.48	0.48	0.43	0.25
Ba	151	103	196	363	239	232	487	321
Rb	14.2	12.3	32.3	76.6	41.9	44.2	186	41.1
Th	1.2	<0.1	3.6	6.8	4.9	3.6	16.5	3.5
Nb	5.7	3	3.6	6.7	5.7	5.1	8.4	5.3
Sr	430	204	160	273	244	201	286	357
Hf	<10	<10	<10	<10	<10	<10	<10	<10
Ti	0.77	0.51	0.46	0.56	0.4	0.37	0.3	0.29
Y	18.7	17.7	21.2	29.8	28.5	27	28.7	15.1

Rock type	Granodiorites				Granites	
Sample	FL-16-7	FL-16-12	FL-16-14	FL-16-15	FL-16-3	FL-16-16
SiO_2	66.92	65.17	67.26	67.6	74.32	70.73
TiO_2	0.47	0.67	0.4	0.44	-	0.32
Al_2O_3	16.15	15.16	15.58	15.58	12.94	14.58
Fe_2O_3	4.33	2.95	2.23	4.55	1.55	3.62
MgO	1.74	2.06	1.27	1.58	0.31	1.02
MnO	0.073	0.11	0.08	0.093	0.03	0.081
CaO	4.11	4.62	4.03	4.24	1.48	3.01
Na_2O	4.34	3.39	3.47	3.58	3.28	3.47
K_2O	1.57	2.35	2.59	2.24	4.12	2.72
P_2O_5	0.13	0.13	0.15	0.11	0.04	0.09
Co_3O_4	<0.005	-	-	<0.005	<0.005	<0.005
CuO	0.021	-	-	0.007	<0.005	<0.005
NiO	<0.003	-	-	<0.003	<0.003	<0.003
Cr_2O_3	<0.01	-	-	<0.01	<0.01	<0.01
V_2O_5	0.012	-	-	0.01	<0.003	0.003
LOI	0.58	0.75	0.75	0.39	0.8	0.46
Total	100.4	99.36	99.45	100.4	99.04	100.1
La	16	15.7	20.9	20.6	37.2	21.7
Ce	32.9	35.2	45	41.4	62.9	42.1
Pr	4.1	4.6	6	5.2	8.7	4.5
Nd	16.2	18.8	22	19.4	30.38	18.1
Sm	2.8	4.5	4.9	3.8	5	3.2
Eu	0.9	1.1	1	1	0.7	0.7
Gd	2.8	4.9	4.8	4	5	3.1
Tb	0.4	0.9	0.8	0.6	0.8	0.5
Dy	2.2	5.4	4.3	3.7	4.5	2.5
Ho	0.5	1.2	0.9	0.9	1	0.6
Er	1.6	3.6	2.6	2.4	3	1.6
Tm	0.2	0.5	0.4	0.4	0.4	0.3
Yb	1.4	3.4	2.3	2.3	2.7	1.4

(*continued on next page*)

Please cite this article in press as: Rodríguez, N., et al., The significance of U–Pb zircon ages in zoned plutons– the case of the Flamenco pluton, Coastal Range batholith, northern Chile, Geoscience Frontiers (2018), https://doi.org/10.1016/j.gsf.2018.06.003

Table 1 (*continued*)

Rock type	Granodiorites				Granites	
Sample	FL-16-7	FL-16-12	FL-16-14	FL-16-15	FL-16-3	FL-16-16
Lu	0.25	-	-	0.47	0.49	0.28
Ba	341	328	373	368	515	443
Rb	41.2	78.7	100	84.1	186	131
Th	3.5	5.2	7.8	10.4	26.9	11.3
Nb	5.2	5.4	7.5	6.4	7.8	6.6
Sr	361	147	123	225	139	162
Hf	<10	<10	<10	<10	<10	<10
Ti	0.28	0.36	0.16	0.26	0.09	0.19
Y	15.2	36.1	26.8	24.4	31.6	13

are observed in the modified alkali-lime index (MALI) (=$Na_2O + K_2O$–CaO) and Fe# (=FeO/(FeO + MgO)) values for the granodiorites (Fig. 3c,d). Flamenco intrusives belong to volcanic arc granitoids (VAG) based on the Nb vs. Y tectonic discrimination diagram (Pearce et al., 1984) (Fig. 3f). Harker variation diagrams (Fig. 4) show these linear trends, defined by the decrease of TiO_2, Al_2O_3, FeO, MgO and CaO and the increase of Na_2O and K_2O contents with increasing SiO_2 from Qtz-diorites to granites. More scattered results are observed in Na_2O and K_2O contents for the granodiorites. Gabbroic samples show the lowest SiO_2 (47.8 wt.% and 48 wt.%) and alkalis contents and the highest values for the rest of the major elements. Nevertheless, sample FL-16-1 presents atypical low FeO and MgO contents for gabbroic compositions (Table 1), probably related to alteration processes that affected the ferromagnesian mineral phases. Generally speaking, Flamenco samples match the compositional trends followed by typical calc-alkaline Cordilleran-type batholiths (Rodríguez et al., 2016) (Figs. 3,4).

The pseudoternary system defined by Opx-An-Or (Díaz-Alvarado et al., 2011; Castro, 2013), the CaO vs. MgO and the molar $K_2O/(K_2O + CaO)$ vs. MgO diagrams, are presented in Fig. 5. These diagrams are particularly illustrative for visualizing magmatic processes as the differentiation of co-genetic granitic rocks. The Opx-An-Or (Fig. 5a) and the CaO vs. MgO (Fig. 5b) projections show an almost linear cotectic-like evolution for the Flamenco intrusives. Higher departures from the linear trends are observed in the granodiorites that show more variable K_2O contents (Fig. 5c). This has been previously related to the local short-range assimilation of pelitic rocks in granodioritic magmas close to the contacts with the host-rocks (Rodríguez et al., 2016).

REE contents highlight differences between magmatic facies and between samples collected from the different areas of the Flamenco pluton. Gabbros show dissimilar results (Fig. 6a). Two gabbroic samples present a positive Eu anomaly, but the FeO- and MgO-depleted sample (FL-16-1 sample) shows higher light rare earth elements (LREE) contents. The Qtz-diorite (FL-16-11) displays an almost flat REE pattern, slightly enriched relative to the gabbro (FL-16-13), and shows an Eu anomaly close to the unity (Fig. 6a). From the Qtz-diorite sample, tonalites (Fig. 6b), granodiorites (Fig. 6c) and granites (Fig. 6e) show a progressive enrichment in LREE and the deepening of the Eu anomaly. The heavy rare earth elements (HREE) values show only slight variations between most samples. A notable difference with this behavior is observed in the SW granodiorites (FL-16-6 and 7). These samples show a significant depletion in HREE and the Eu anomaly is almost absent (Fig. 6c). These characteristics can be easily observed in a $(La/Yb)_N$ vs. $(Eu/^*Eu)_N$ diagram (Fig. 6e). The La/Yb values increase and the REE display steeper patterns as the Eu contents and the $(Eu/^*Eu)_N$ ratio decrease for most of the studied samples of the Flamenco pluton. However, SW granodiorites show the highest $(La/Yb)_N$ ratios and Sr values among the granodiorites, and $(Eu/^*Eu)_N$ ratios close to the unity (Fig. 6e). These characteristics involve the departure of these rocks from the trend defined by the rest of the Flamenco samples. Further, this area of the pluton contains granodiorites with the highest Sr/Y ratios among the studied samples, which fall in the low Y field of the Sr/Y vs. Y diagram (Fig. 6f).

Regarding to the spider diagrams (Fig. 7), gabbroic samples show different values for mobile elements and LREE and more similar results for HREE. Qtz-diorites to tonalites present similar patterns with progressive enrichment in mobile elements (Ba, Rb, Th and K) and more pronounced Nb, Sr and Ti anomalies. In general, the Flamenco intrusives show trace elements contents similar to the typical arc setting magmatism (Kelemen et al., 2003).

5.2. Zircons description and SHRIMP U–Pb geochronological results

The U–Pb zircon geochronology results of the eight studied samples (Fig. 1c) are described together with the morphological characteristics of the zircon populations and Th and U contents. According to the scattering of ages in most samples, between 9 Myr and 41 Myr, we have calculated the average ages of groups of geochronological data based on the U–Pb ages and the morphological similarities between zircon crystals and internal structures (composition, zonation, etc). The geological significance of mean concordia ages and individual ages will be discussed in the context of the geochemical characteristics and field relations found in the magmatic facies that comprise the Flamenco pluton. Concordia and weighted mean diagrams are presented in Fig. 8 together with images of zircon crystals representative of the different crystal typologies contained in zircon populations. The images of the zircon populations separated in each sample are provided in the Supplementary material. U–Pb geochronology data are given in Table 2.

5.2.1. Gabbro FL-16-1

This sample is a fine-to medium-grained melanocratic rock that displays inequigranular, phaneritic, hypidiomorphic and poikilitic textures. Mineralogical composition is dominated by subhedral to anhedral twinned (simple and polysynthetic) Pl crystals (~65 vol.%) with a grain size of 0.75–2.5 mm. Plagioclase crystals are weakly altered to sericite and epidote. Subhedral Hbl crystals (~30 vol.%) with a grain size of 0.14–2.5 mm are moderately altered to Fe-rich Chl and Ep. Opx is present in the inner areas of Hbl aggregates. A minor proportion of subhedral secondary Bt crystals (~5 vol.%) with a grain size of 0.5–2.75 mm are also present. Opaque minerals including Sph represent less than 2 vol.%. Poikilitic textures are observed in the gabbros where Hbl encloses small Pl crystals.

Sample FL-16-1 contains mostly coarse around 500 μm long zircon crystals, and few smaller zircon grains (~5%, 200 μm long crystals) (Fig. 8a). Morphologically, they can be subdivided into two groups. A first group (~30%) presents euhedral to subhedral

Please cite this article in press as: Rodríguez, N., et al., The significance of U–Pb zircon ages in zoned plutons– the case of the Flamenco pluton, Coastal Range batholith, northern Chile, Geoscience Frontiers (2018), https://doi.org/10.1016/j.gsf.2018.06.003

Table 2
U–Th–Pb results for the Flamenco pluton magmatic facies.

Spot	$^{206}Pb_c$ (%)	U (ppm)	Th (ppm)	$^{206}Pb^*$ (ppm)	$^{232}Th/^{238}U$	$^{206}Pb/^{238}U$ Age[a]	$^{207}Pb/^{206}Pb$ Age[a]	$^{207}Pb^*/^{206}Pb^*$[a]	±%	$^{207}Pb^*/^{235}U$[a]	±%	$^{206}Pb^*/^{238}U$[a]	±%	err corr
a: Summary of SHRIMP U–Pb zircon data for FL-16-1 gabbros														
1.1	0.60	122	124	3.3	1.05	198±5	210±134	0.0503	5.8	0.22	6.3	0.031	2.4	0.4
1.2	3.23	63	27	1.7	0.43	197±6	221±411	0.0506	17.8	0.22	18.0	0.031	3.0	0.2
2.1	0.95	129	142	3.3	1.14	190±5	225±153	0.0507	6.6	0.21	7.2	0.030	2.8	0.4
3.1	0.98	72	72	1.9	1.04	194±5	223±207	0.0506	8.9	0.21	9.3	0.031	2.4	0.3
4.1	0.30	170	184	4.4	1.12	191±5	153±101	0.0491	4.3	0.20	5.1	0.030	2.8	0.5
5.1	0.96	87	63	2.3	0.75	193±6	167±209	0.0494	8.9	0.21	9.5	0.030	3.3	0.3
6.1	0.20	164	212	4.2	1.34	189±4	161±91	0.0493	3.9	0.20	4.5	0.030	2.2	0.5
7.1	1.07	107	114	2.6	1.10	180±7	186±232	0.0498	10.0	0.19	10.7	0.028	3.8	0.4
8.1	1.29	123	122	3.2	1.03	192±4	145±219	0.0489	9.3	0.20	9.6	0.030	2.3	0.2
9.1	1.81	85	95	2.2	1.16	194±5	214±283	0.0504	12.2	0.21	12.5	0.031	2.7	0.2
10.1	0.87	178	104	4.6	0.60	191±5	198±141	0.0501	6.1	0.21	6.7	0.030	2.8	0.4
11.1	0.64	196	229	5.2	1.21	198±5	312±94	0.0526	4.1	0.23	4.8	0.031	2.5	0.5
12.1	0.63	181	226	4.8	1.29	198±5	157±138	0.0492	5.9	0.21	6.5	0.031	2.7	0.4
12.2	0.90	234	90	5.9	0.40	187±5	159±142	0.0492	6.1	0.20	6.6	0.029	2.6	0.4
13.1	0.76	154	177	3.9	1.19	186±5	252±134	0.0512	5.8	0.21	6.4	0.029	2.7	0.4
13.2	3.38	48	19	1.2	0.41	183±6	214±562	0.0504	24.3	0.20	24.5	0.029	3.5	0.1
14.1	0.78	117	117	3.0	1.04	189±4	175±194	0.0496	8.3	0.20	8.6	0.030	2.3	0.3
15.1	1.37	95	106	2.5	1.14	196±8	165±263	0.0494	11.3	0.21	12.0	0.031	4.2	0.3
16.1	0.64	189	206	5.0	1.13	195±5	320±87	0.0528	3.8	0.22	4.6	0.031	2.6	0.6
17.1	1.41	108	130	2.6	1.24	180±5	278±215	0.0518	9.4	0.20	9.8	0.028	2.7	0.3
b: Summary of SHRIMP U–Pb zircon data for FL-16-2 granodiorites														
1.1	1.19	68	53	1.8	0.81	196±5	241±208	0.0510	9.0	0.217	9.4	0.0308	2.7	0.3
2.1	0.35	176	119	4.5	0.70	191±5	149±118	0.0490	5.0	0.203	5.8	0.0301	2.9	0.5
3.1	2.06	52	32	1.4	0.64	194±6	307±306	0.0525	13.4	0.221	13.8	0.0305	3.2	0.2
4.1	0.78	233	154	6.3	0.68	200±5	256±88	0.0513	3.8	0.224	4.6	0.0316	2.5	0.5
4.2	0.90	124	69	3.0	0.58	182±4	195±156	0.0500	6.7	0.198	7.1	0.0287	2.4	0.3
5.1	0.22	309	181	8.3	0.60	199±5	115±74	0.0483	3.1	0.208	4.0	0.0313	2.5	0.6
5.2	0.65	232	275	6.0	1.22	193±5	384±50	0.0543	2.2	0.227	3.5	0.0303	2.7	0.8
6.1	1.48	76	63	1.9	0.86	185±5	100±269	0.0480	11.4	0.193	11.7	0.0291	2.5	0.2
7.1	1.69	58	52	1.5	0.93	194±6	322±243	0.0528	10.7	0.222	11.1	0.0305	3.1	0.3
7.2	0.29	772	450	19.2	0.60	184±5	179±39	0.0497	1.7	0.198	3.0	0.0289	2.5	0.8
8.1	2.23	110	130	2.7	1.22	183±5	225±246	0.0507	10.7	0.201	11.0	0.0288	2.8	0.3
8.2	1.87	110	82	2.8	0.77	186±5	61.1±317	0.0472	13.3	0.191	13.5	0.0293	2.5	0.2
9.1	1.49	101	96	2.6	0.98	188±5	149±230	0.0490	9.8	0.200	10.2	0.0296	2.9	0.3
9.2	0.94	325	196	7.8	0.62	178±5	158±130	0.0492	5.6	0.190	6.4	0.0280	3.1	0.5
10.1	0.99	117	38	12.7	0.34	770±21	905±51	0.0692	2.5	1.211	3.8	0.1269	2.9	0.8
10.2	0.94	170	96	4.5	0.58	193±5	120±157	0.0484	6.7	0.203	7.2	0.0305	2.6	0.4
11.1	2.63	59	60	1.5	1.04	187±5	132±402	0.0487	17.1	0.198	17.3	0.0295	2.7	0.2
12.1	3.44	83	58	2.1	0.73	188±5	296±324	0.0523	14.2	0.214	14.5	0.0297	3.0	0.2
13.1	0.62	219	172	5.5	0.81	185±5	81.6±122	0.0476	5.1	0.191	5.7	0.0291	2.5	0.4
14.1	1.48	110	122	2.8	1.15	186±5	273±178	0.0517	7.8	0.209	8.2	0.0293	2.6	0.3
15.1	0.35	296	395	7.7	1.38	192±5	101±86	0.0480	3.6	0.200	4.6	0.0302	2.9	0.6
16.1	0.49	187	163	4.7	0.90	187±4	45.2±155	0.0469	6.5	0.191	6.9	0.0294	2.3	0.3
c: Summary of SHRIMP U–Pb zircon data for FL-16-6 granodiorites														
1.1	0.24	96	59	2.9	0.64	223±7	114±164	0.0483	7.0	0.235	7.6	0.0353	3.1	0.4
2.1	0.62	172	160	5.1	0.96	220±5	29.9±163	0.0466	6.8	0.223	7.2	0.0347	2.4	0.3
3.1	0.82	118	67	3.3	0.59	209±6	344±100	0.0534	4.4	0.242	5.2	0.0329	2.8	0.5
4.1	0.65	148	102	4.3	0.71	215±5	579±77	0.0593	3.6	0.277	4.3	0.0339	2.4	0.6
5.1	–	390	159	62.7	0.42	1106±26	1093±10	0.0759	0.5	1.959	2.6	0.1871	2.5	1.0
5.2	0.82	119	76	3.4	0.66	209±5	103±178	0.0481	7.5	0.218	7.9	0.0329	2.4	0.3
6.1	0.60	148	107	4.2	0.75	209±7	296±85	0.0522	3.7	0.238	5.1	0.0330	3.5	0.7
7.1	1.07	49	36	1.4	0.77	217±6	192±263	0.0499	11.3	0.235	11.6	0.0342	2.6	0.2
8.1	0.42	261	320	7.6	1.27	213±5	35.9±108	0.0467	4.5	0.217	5.2	0.0336	2.6	0.5
9.1	1.47	104	62	3.0	0.61	211±6	301±172	0.0524	7.6	0.240	8.0	0.0332	2.7	0.3
10.1	0.70	142	95	4.1	0.69	213±5	181±131	0.0497	5.6	0.230	6.1	0.0336	2.4	0.4
11.1	0.71	161	120	4.7	0.77	214±5	82.8±150	0.0477	6.3	0.222	6.8	0.0337	2.6	0.4
12.1	2.20	55	28	1.6	0.53	216±7	222±322	0.0506	13.9	0.238	14.3	0.0341	3.1	0.2
12.1	1.25	109	57	3.2	0.54	216±5	319±146	0.0528	6.4	0.248	6.9	0.0341	2.4	0.3
13.1	0.65	165	115	4.8	0.72	213±5	148±121	0.0490	5.2	0.227	5.7	0.0336	2.5	0.4
14.1	1.92	52	39	1.4	0.76	202±6	297±275	0.0523	12.0	0.229	12.4	0.0318	3.1	0.3
d: Summary of SHRIMP U–Pb zircon data for FL-16-11 Qtz-diorites														
1.1	0.28	328	137	8.3	0.43	188±5	245±60	0.0511	2.6	0.208	3.7	0.0295	2.6	0.7
2.1	0.53	134	109	3.5	0.84	193±4	122±137	0.0485	5.8	0.203	6.3	0.0303	2.4	0.4
3.1	0.48	135	123	3.4	0.94	186±6	151±123	0.0491	5.2	0.198	6.2	0.0293	3.2	0.5
4.1	0.77	118	84	3.0	0.74	190±5	109±169	0.0482	7.2	0.199	7.7	0.0300	2.8	0.4
5.1	0.73	123	107	3.1	0.90	187±6	98.9±167	0.0480	7.0	0.195	7.7	0.0295	3.1	0.4
6.1	2.03	55	29	1.4	0.54	191±8	133±397	0.0487	16.9	0.202	17.4	0.0300	4.1	0.2
7.1	0.80	100	73	2.6	0.76	192±7	102±197	0.0481	8.3	0.201	9.0	0.0303	3.4	0.4
7.2	0.86	153	58	3.9	0.39	186±5	162±144	0.0493	6.2	0.199	6.8	0.0292	2.7	0.4
8.1	2.69	61	29	1.6	0.49	191±5	279±323	0.0519	14.1	0.215	14.4	0.0300	2.8	0.2
8.2	0.59	133	118	3.4	0.92	186±5	51.5±168	0.0470	7.0	0.190	7.6	0.0293	2.8	0.4

(*continued on next page*)

Please cite this article in press as: Rodríguez, N., et al., The significance of U–Pb zircon ages in zoned plutons– the case of the Flamenco pluton, Coastal Range batholith, northern Chile, Geoscience Frontiers (2018), https://doi.org/10.1016/j.gsf.2018.06.003

Table 2 (*continued*)

Spot	$^{206}Pb_c$ (%)	U (ppm)	Th (ppm)	$^{206}Pb^*$ (ppm)	$^{232}Th/^{238}U$	$^{206}Pb/^{238}U$ Age[a]	$^{207}Pb/^{206}Pb$ Age[a]	$^{207}Pb^*/^{206}Pb^*$[a]	±%	$^{207}Pb^*/^{235}U$[a]	±%	$^{206}Pb^*/^{238}U$[a]	±%	err corr
9.1	1.47	90	68	2.3	0.78	194±6	276±211	0.0518	9.2	0.218	9.8	0.0305	3.4	0.3
9.2	1.77	65	35	1.6	0.56	186±5	449±265	0.0559	11.9	0.226	12.3	0.0293	2.8	0.2
10.1	0.72	188	121	4.8	0.66	190±5	363±69	0.0538	3.1	0.222	4.2	0.0299	2.8	0.7
11.1	1.15	112	78	2.8	0.72	187±5	249±170	0.0512	7.4	0.208	7.9	0.0294	2.8	0.4
12.1	1.02	152	139	3.9	0.95	189±6	79.6±185	0.0476	7.8	0.195	8.3	0.0297	3.0	0.4
13.1	0.92	128	109	3.3	0.88	191±5	384±123	0.0543	5.5	0.226	6.0	0.0301	2.4	0.4
14.1	1.00	113	95	2.8	0.87	185±5	161±195	0.0493	8.3	0.198	8.8	0.0292	2.9	0.3
15.1	1.29	150	63	3.7	0.43	185±5	232±172	0.0508	7.4	0.203	8.0	0.0290	2.9	0.4
e: Summary of SHRIMP U–Pb zircon data for FL-16-12 granodiorites														
1.1	1.62	89	86	2.3	1.00	192±6	181±232	0.04970	10	0.2077	10	0.0303	3.1	0.30
2.1	0.27	314	168	13.4	0.55	312±7	354±35	0.05358	2	0.3662	3	0.0496	2.3	0.82
2.2	0.51	266	223	12.0	0.87	329±6	298±64	0.05228	3	0.3772	3	0.0523	2.0	0.58
2.3	3.15	112	55	3.0	0.51	200±4	199±338	0.05008	15	0.2176	15	0.0315	2.1	0.15
3.1	2.32	229	88	82.5	0.40	2299±34	2482±24	0.16249	1	9.6019	2	0.4286	1.7	0.78
3.2	1.60	131	82	3.8	0.64	215±3	232±221	0.05080	10	0.2376	10	0.0339	1.7	0.17
4.1	0.17	323	92	20.4	0.30	459±9	521±19	0.05776	1	0.5881	2	0.0738	1.9	0.91
4.2	1.85	120	62	3.6	0.54	221±4	232±203	0.05081	9	0.2447	9	0.0349	1.7	0.19
5.1	0.31	248	84	21.3	0.35	615±9	620±29	0.06045	1	0.8350	2	0.1002	1.5	0.74
5.2	1.94	122	69	3.3	0.58	198±4	236±230	0.05089	10	0.2191	10	0.0312	2.1	0.21
6.1	0.35	187	76	27.3	0.42	1016±17	1057±17	0.07457	1	1.7545	2	0.1706	1.9	0.91
7.1	5.38	129	113	3.5	0.90	201±5	247±379	0.05113	16	0.2232	17	0.0317	2.7	0.16
7.2	7.19	94	60	2.9	0.67	228±8	241±813	0.05101	35	0.2531	35	0.0360	3.8	0.11
8.1	3.19	96	83	2.5	0.89	194±3	241±303	0.05101	13	0.2152	13	0.0306	1.8	0.14
8.2	1.20	210	122	5.9	0.60	206±3	218±139	0.05049	6	0.2262	6	0.0325	1.7	0.27
9.1	3.51	90	62	2.3	0.71	190±4	217±389	0.05049	17	0.2081	17	0.0299	2.2	0.13
10.1	3.61	50	34	1.3	0.70	190±4	270±457	0.05165	20	0.2126	20	0.0299	2.1	0.11
11.1	5.47	63	46	1.6	0.75	183±4	206±524	0.05023	23	0.2000	23	0.0289	2.2	0.10
12.1	2.52	152	75	3.9	0.51	191±4	214±254	0.05041	11	0.2090	11	0.0301	2.0	0.18
13.1	0.80	226	275	5.8	1.26	192±4	176±109	0.04960	5	0.2063	5	0.0302	2.0	0.40
14.1	1.75	202	207	5.3	1.05	192±3	202±164	0.05016	7	0.2093	7	0.0303	1.6	0.22
14.2	8.73	168	75	6.6	0.46	288±10	238±874	0.05094	38	0.3208	38	0.0457	3.4	0.09
15.1	2.07	82	55	2.1	0.69	192±4	220±297	0.05053	13	0.2104	13	0.0302	2.2	0.17
f: Summary of SHRIMP U–Pb zircon data for FL-16-15 granodiorites														
1.1	1.37	97	88	2.5	0.93	190±5	223±224	0.0506	9.7	0.21	10.0	0.030	2.4	0.2
2.1	0.16	237	208	6.0	0.91	188±4	290±62	0.0521	2.7	0.21	3.5	0.030	2.2	0.6
2.2	0.73	289	144	7.9	0.51	201±4	180±108	0.0497	4.6	0.22	5.1	0.032	2.2	0.4
3.1	1.54	90	51	2.3	0.58	189±5	211±260	0.0504	11.2	0.21	11.5	0.030	2.8	0.2
4.1	1.02	175	103	4.3	0.61	183±5	260±142	0.0514	6.2	0.20	6.8	0.029	2.9	0.4
4.2	0.66	391	247	11.9	0.65	224±5	175±116	0.0496	5.0	0.24	5.4	0.035	2.2	0.4
5.1	1.63	103	56	2.6	0.55	186±4	142±291	0.0489	12.4	0.20	12.6	0.029	2.4	0.2
5.2	0.82	210	118	5.6	0.58	197±5	303±103	0.0524	4.5	0.22	5.1	0.031	2.3	0.5
6.1	3.48	77	66	2.0	0.88	189±5	263±465	0.0515	20.2	0.21	20.4	0.030	2.6	0.1
6.2	1.18	148	87	3.8	0.61	191±4	167±206	0.0494	8.8	0.21	9.1	0.030	2.3	0.3
7.1	0.65	144	73	3.7	0.52	192±4	168±147	0.0494	6.3	0.21	6.7	0.030	2.3	0.3
8.1	0.38	412	647	10.7	1.62	191±5	167±73	0.0494	3.1	0.20	4.1	0.030	2.7	0.7
9.1	0.51	295	145	7.7	0.51	192±5	162±115	0.0493	4.9	0.21	5.6	0.030	2.6	0.5
10.1	0.51	348	294	9.1	0.87	193±5	261±69	0.0514	3.0	0.22	3.8	0.030	2.4	0.6
11.1	0.82	288	187	7.6	0.67	196±5	279±116	0.0519	5.1	0.22	5.8	0.031	2.9	0.5
12.1	0.82	272	223	7.1	0.85	195±4	473±43	0.0565	1.9	0.24	3.0	0.031	2.3	0.8
13.1	1.30	345	218	10.3	0.65	220±5	179±191	0.0497	8.2	0.24	8.5	0.035	2.2	0.3
14.1	0.64	238	244	6.4	1.06	200±5	294±112	0.0522	4.9	0.23	5.5	0.032	2.4	0.4
15.1	0.99	361	248	10.2	0.71	208±5	177±123	0.0496	5.3	0.22	5.7	0.033	2.2	0.4
16.1	0.92	291	203	7.9	0.72	202±5	173±117	0.0495	5.0	0.22	5.7	0.032	2.7	0.5
g: Summary of SHRIMP U–Pb zircon data for ME-16-2 porphyritic dyke														
1.1	2.47	69	29	1.9	0.44	198±4	226±308	0.05067	13	0.2181	13	0.0312	1.9	0.14
2.1	1.67	88	41	2.4	0.48	199±3	188±263	0.04985	11	0.2153	11	0.0313	1.7	0.15
3.1	4.38	77	28	2.0	0.37	196±4	223±409	0.05061	18	0.2150	18	0.0308	2.0	0.11
4.1	1.77	69	25	2.0	0.38	214±4	236±249	0.05089	11	0.2365	11	0.0337	1.8	0.16
5.1	2.25	60	19	1.6	0.32	200±4	189±386	0.04988	17	0.2167	17	0.0315	1.9	0.11
6.1	3.30	57	19	1.5	0.35	191±5	243±383	0.05104	17	0.2111	17	0.0300	2.6	0.15
7.1	1.77	88	37	2.3	0.44	195±3	207±256	0.05027	11	0.2124	11	0.0306	1.8	0.16
8.1	2.97	86	35	2.3	0.42	199±4	242±321	0.05102	14	0.2201	14	0.0313	1.8	0.13
9.1	1.77	92	51	2.4	0.58	198±4	249±241	0.05117	10	0.2199	11	0.0312	2.2	0.21
9.2	3.60	75	33	2.0	0.45	193±4	191±444	0.04991	19	0.2089	19	0.0304	1.9	0.10
10.1	0.19	244	137	27.1	0.58	783±11	796±20	0.06568	1	1.1699	2	0.1292	1.5	0.85
10.2	5.01	58	22	1.6	0.39	202±4	276±489	0.05178	21	0.2275	21	0.0319	2.2	0.10
11.1	5.40	72	34	1.9	0.49	196±6	250±580	0.05120	25	0.2184	25	0.0309	3.3	0.13
12.1	0.81	156	78	4.1	0.52	196±5	265±109	0.05154	5	0.2197	5	0.0309	2.4	0.45
13.1	2.00	94	39	2.5	0.42	196±6	218±260	0.05049	11	0.2152	12	0.0309	2.9	0.25
14.1	1.90	71	26	1.9	0.39	198±5	232±315	0.05080	14	0.2189	14	0.0312	2.3	0.17
h: Summary of SHRIMP U–Pb zircon data for FL-16-4 metasediments														
1.1	0.20	116	52	20.6	0.46	1206±30	1102±34	0.0762	1.7	2.16	3.2	0.206	2.7	0.8
2.1	0.27	285	55	31.6	0.20	784±26	818±40	0.0664	1.9	1.18	4.0	0.129	3.6	0.9
3.1	0.33	203	73	15.5	0.37	548±14	457±53	0.0561	2.4	0.69	3.5	0.089	2.6	0.7

Please cite this article in press as: Rodríguez, N., et al., The significance of U–Pb zircon ages in zoned plutons– the case of the Flamenco pluton, Coastal Range batholith, northern Chile, Geoscience Frontiers (2018), https://doi.org/10.1016/j.gsf.2018.06.003

Table 2 (*continued*)

Spot	$^{206}Pb_c$ (%)	U (ppm)	Th (ppm)	$^{206}Pb^*$ (ppm)	$^{232}Th/^{238}U$	$^{206}Pb/^{238}U$ Age[a]	$^{207}Pb/^{206}Pb$ Age[a]	$^{207}Pb^*/^{206}Pb^*$[a]	±%	$^{207}Pb^*/^{235}U$[a]	±%	$^{206}Pb^*/^{238}U$[a]	±%	err corr
3.2	2.43	1561	151	43.0	0.10	204±5	244±149	0.0511	6.5	0.23	6.9	0.032	2.4	0.3
4.1	0.22	342	71	25.7	0.21	540±12	536±28	0.0582	1.3	0.70	2.6	0.087	2.3	0.9
5.1	0.18	342	200	26.4	0.60	554±14	547±61	0.0585	2.8	0.72	3.9	0.090	2.7	0.7
5.2	0.53	377	109	25.6	0.30	493±12	619±74	0.0604	3.4	0.66	4.3	0.079	2.6	0.6
6.1	0.57	338	36	23.5	0.11	499±11	415±74	0.0551	3.3	0.61	4.0	0.081	2.3	0.6
6.2	3.43	406	54	36.9	0.14	670±33	1383±156	0.0880	8.1	1.33	9.7	0.110	5.2	0.5
7.1	0.07	447	58	62.1	0.13	966±21	953±12	0.0709	0.6	1.58	2.4	0.162	2.3	1.0
7.2	0.70	668	10	33.0	0.02	360±9	338±54	0.0532	2.4	0.42	3.5	0.057	2.6	0.7
8.1	0.88	111	58	14.7	0.54	931±24	1032±35	0.0737	1.7	1.58	3.3	0.155	2.8	0.8
9.1	1.85	444	124	87.4	0.29	1350±28	1615±11	0.0995	0.6	3.20	2.4	0.233	2.3	1.0
10.1	2.11	185	49	15.2	0.27	594±23	857±55	0.0676	2.6	0.90	4.9	0.096	4.1	0.8
11.1	0.89	275	29	30.3	0.11	782±26	955±43	0.0709	2.1	1.26	4.1	0.129	3.5	0.9
12.1	0.97	97	36	13.7	0.39	984±21	1071±38	0.0751	1.9	1.71	3.0	0.165	2.3	0.8
13.1	1.12	129	32	14.9	0.26	816±26	999±69	0.0725	3.4	1.35	4.8	0.135	3.4	0.7
13.2	10.10	807	16	24.9	0.02	228±5	280±404	0.0519	17.7	0.26	17.8	0.036	2.4	0.1
14.1	0.60	457	119	33.5	0.27	529±11	571±33	0.0591	1.5	0.70	2.7	0.086	2.3	0.8
14.2	1.65	737	251	45.5	0.35	448±10	512±62	0.0575	2.8	0.57	3.7	0.072	2.4	0.6

Errors are 1-sigma; Pb_c and Pb^* indicate the common and radiogenic portions, respectively.
Error in Standard calibration was 0.53% for samples FL-16-1, -4, -12, -15 and ME-16-2 and 0.68% for samples FL-16-2, -6 and -11.
(not included in above errors but required when comparing data from different mounts).
[a] Common Pb corrected using measured ^{204}Pb.

crystals and crystal fragments with high aspect ratios (5:1) and parallel banded zonation (e.g. zircons 3, 8, 15, Supplementary material). Pyramidal tips are almost absent in these acicular zircons. A second group (~70%) is characterized by subhedral rounded crystals with complex internal zonation, some of them present a faint or absent zonation truncated by a high-luminosity irregular external rim (e.g. zircons 4 and 6, Supplementary material) with a lesser amount showing concentric oscillatory zonation. Small crystals are morphologically similar to the larger ones. Th/U ratios are comprised between 1.34 and 1.03, except for high-luminosity rims with Th/U ranging from 0.40 to 0.43 (Table 2). The complex inner area of a rounded zircon and a small crystal presents Th/U ratios of 0.75 and 0.60 respectively.

Twenty analyses yield $^{206}Pb/^{238}U$ ages between 198 Ma and 180 Ma giving a mean age of 191 ± 2.3 Ma (MSWD = 1.14; Probability = 0.30; Fig. 8a). Detailed analysis of these results show three groups according to their morphological characteristics and $^{206}Pb/^{238}U$ ages: an older group gives the same age within analytical uncertainty ($N = 12$; MSWD = 0.67; Probability = 0.41), giving a concordia age of 194.7 ± 1.5 Ma, and includes most of the analyses of large acicular crystals and the inner area of rounded zircons. A younger cluster of analyses that includes rounded zircons (inner areas and high-luminosity overgrowths) yields a concordia age of 188.3 ± 2.1 Ma ($N = 5$; MSWD = 0; Probability = 0.99). The three youngest ages between 183 and 180 Ma are analyzed in two small zircons and an external rim (Table 2, Fig. 8a).

5.2.2. Granodiorite FL-16-2

FL-16-2 sample is a mesocratic rock that exhibits a phaneritic, hypidiomorphic, inequigranular and poikilitic textures. The mineralogical composition is dominated by anhedral Qtz (~40 vol.%) that shows a grain size between 0.07 mm and 2.05 mm, euhedral to subhedral Pl (~25 vol.%) strongly altered to sericite with a grain size of 0.29–1.3 mm, subhedral Bt (~20 vol.%) ranging from 1.4 mm to 5.5 mm, suhedral to anhedral sericitized Kfs crystals (~15 vol.%) with a grain size of 0.44–0.73 mm and 0.14 mm to 0.88 mm anhedral Hbl (~5 vol.%).

The zircon population of the FL-16-2 sample is dominated by euhedral to subhedral equant and low aspect ratio (2:1) crystals with both pyramidal and flat tips. They mostly present a high-luminosity inner area with diffuse or concentric zonation pattern. Some of them show an external overgrowth (e.g. zircons 2, 7 and 9, Supplementary material) with concentric oscillatory zoning that mimics the shape of the inner area. A few simple acicular crystals of variable grain size (500–200 μm long) are also present (e.g. zircons 13, 14 and 16, Supplementary material). Th/U ratios are comprised between 0.58 and 1.38, although the most abundant zircon population presents Th/U ratios between 0.58 and 0.9 (Table 2).

An inherited core gives a Neoproterozoic age (10.1: 770 ± 21 Ma, Table 2). Omitting the oldest age, the remaining 21 analyses yield the same age within analytical uncertainty (MSWD = 1.23; Probability = 0.21), giving a weighted mean $^{206}Pb/^{238}U$ age of 188.7 ± 2.1 Ma (Fig. 8b). The resulting analyses can be divided into two older ages around 200 Ma, one of them was found in an external rim with an apparent younger core (zircon 4, Fig. 8b); an older cluster mostly comprised by the inner high-luminosity areas of larger zircons that gives the same age within analytical uncertainty ($N = 7$; MSWD = 0.82; Probability = 0.37), giving a concordia age of 193.1 ± 2.2 Ma, and a younger group between 188 and 182 Ma, which is a more heterogeneous group that includes the inner areas of medium-to small-grained crystals and small acicular zircons. This group yields a concordia age of 185.5 ± 1.4 Ma ($N = 11$; MSWD = 0.33; Probability = 0.57). The youngest age of 178 ± 5 Ma was found in an external overgrowth. It is remarkable the presence of zircons with significant age differences (10 Ma) between the inner high-luminosity area and the external overgrowth (zircons 7 and 9, Fig. 8b).

5.2.3. Granodiorite FL-16-6

This is a leucocratic rock with phaneritic and equigranular textures. The mineralogical composition is dominated by anhedral Qtz (~40 vol.%) with a grain size of 0.07–1.3 mm. Twinned euhedral to subhedral Pl crystals (~30 vol.%) show concentric zonation and are weakly altered to sericite. Subhedral to anhedral Hbl crystals (~15 vol.%) range from 0.4 mm to 1.6 mm, subhedral to anhedral large (0.4–2 mm) Bt crystals (~10 vol.%) and, in less proportion, subhedral Kfs crystals (~5 vol.%) conform these rocks. Small opaque and zircon crystals represent the main accessory phases.

Zircon grains collected from the FL-16-6 sample (Supplementary material) are coarse-grained euhedral crystals divided into elongated zircons (above 5:1 aspect ratios and 500 μm long; e.g. 3, 4) and shorter prisms that commonly present an inherited core (2:1 to 3:1 aspect ratios and 100–200 μm long crystals; e.g. 1, 5, 11). All zircons show a prominent concentric zoning in the pyramidal tips of the largest crystals and around an

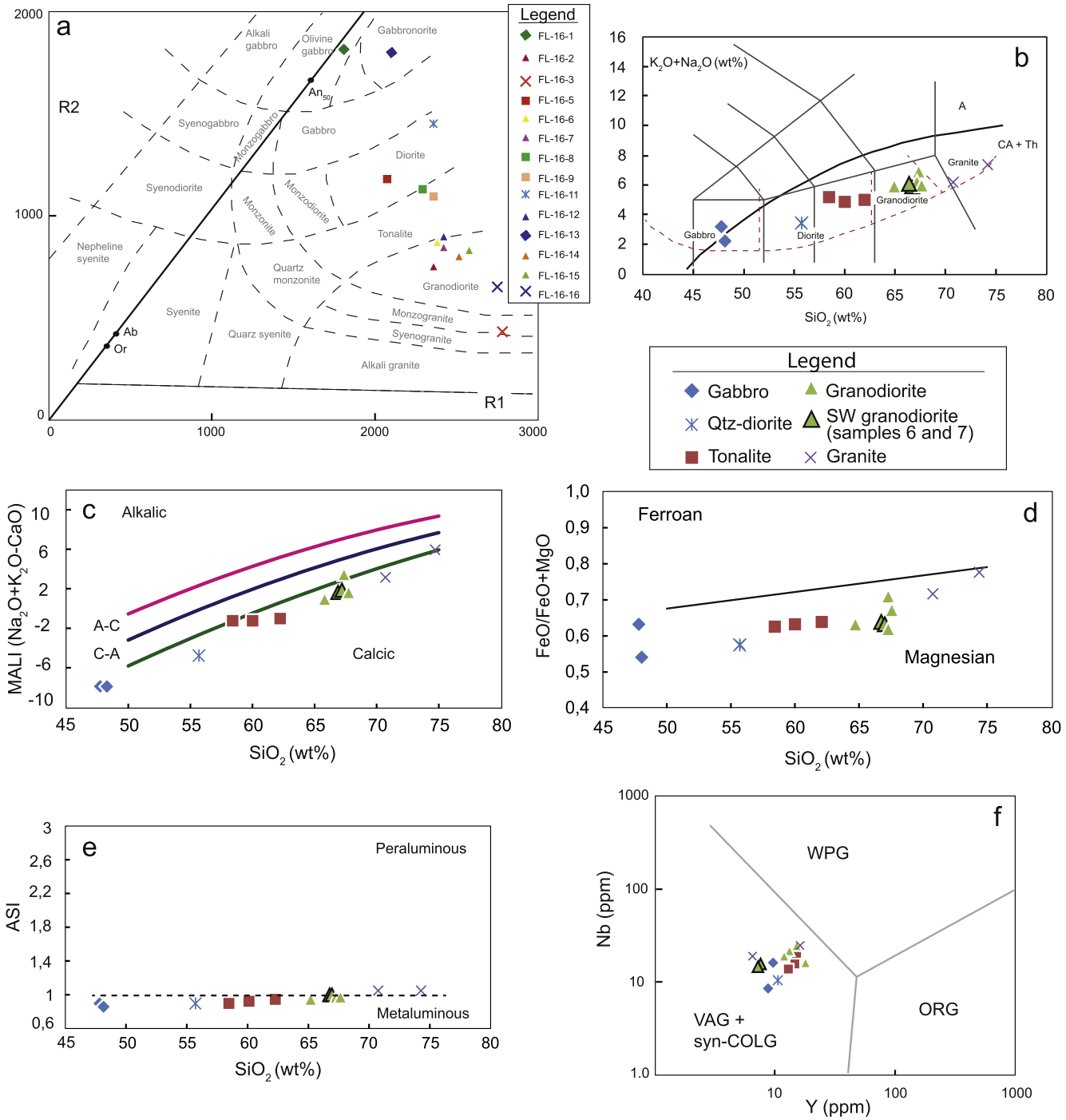

Figure 3. Geochemical classification diagrams. (a) R1 (4Si−11(Na + K)−2(Fe + Ti)) vs. R2 (6Ca+2 Mg + Al) cationic diagram of De La Roche et al. (1980). Major subdivisions and the denomination of the intrusive facies of the Flamenco pluton have been assigned according to this classification. (b) TAS (Total alkalis vs silica) classification diagram (Le Bas et al., 1986). The fields divided by the dashed lines are based on the TAS diagram adaptation for plutonic rocks (Wilson, 1989). The curved solid line separates the alkaline (A) and calc-alkaline/tholeiitic (CA + Th) series. (c) MALI ($Na_2O + K_2O$−CaO), (d) #Fe and (e) Aluminum Saturation Index (ASI) vs. silica granitoid classification diagrams (Frost et al., 2001). (f) Nb−Y tectonic discrimination diagram (Pearce et al., 1984). WPG: Within-plate granite, ORG: Ocean ridge granite, VAR: Volcanic arc granite, Syn-COLG: Syn-collision granite.

apparent inherited core in the smaller and rounded zircon grains (Fig. 8c, Supplementary material). Th/U ratios are comprised between 0.53 and 0.96, excluding an inherited core (0.42) and an analysis of an acicular crystal (1.27) (Table 2).

An inherited core gives a Mesoproterozoic age (5.1: 1106 ± 27 Ma, Table 2). Fifteen $^{206}Pb/^{238}U$ ages are comprised between 223 Ma and 202 Ma and yield the same age within analytical uncertainty (MSWD = 0.84; Probability = 0.62), giving a weighted mean $^{206}Pb/^{238}U$ age of 213.2 ± 2.9 Ma (Fig. 8c). Two older ages (1.1 and 2.1: 220 Ma and 223 Ma) are obtained in a subhedral small zircon and a euhedral crystal with a 3:1 aspect ratio. The main set of analyses is obtained grouping both long and shorter prisms, giving a concordia age of 212.8 ± 3.3 Ma (N = 12; MSWD = 0.24; Probability = 0.99) (Fig. 8c). A younger analysis of a medium-grained elongated crystal yields an age of 202 ± 6 Ma (14.1, Table 2).

Please cite this article in press as: Rodríguez, N., et al., The significance of U–Pb zircon ages in zoned plutons– the case of the Flamenco pluton, Coastal Range batholith, northern Chile, Geoscience Frontiers (2018), https://doi.org/10.1016/j.gsf.2018.06.003

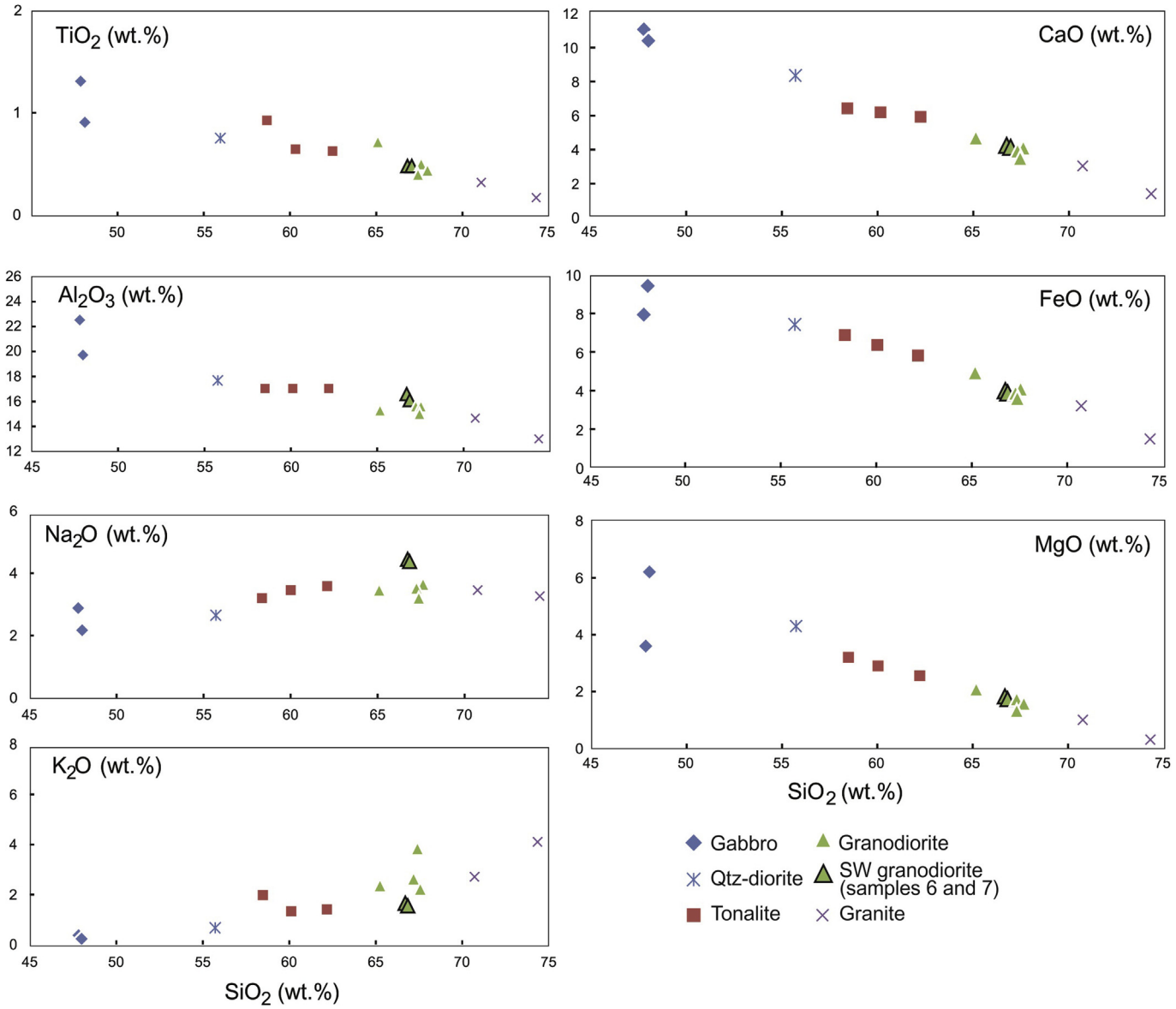

Figure 4. Major element vs. silica variation (Harker) diagrams for the sampled intrusive facies of the Flamenco pluton.

5.2.4. Qtz-diorite FL-16-11

FL-16-11 sample is a mesocratic rock with equigranular, hypidiomorphic, poikilitic and skeletal textures. The mineralogical composition is dominated by euhedral to subhedral Pl crystals (~60 vol.%) 0.25–3 mm in size that are weakly altered to sericite, Hbl (~20 vol.%) with a grain size of 0.5–3.5 mm, anhedral Qtz (~7 vol.%) and subhedral altered Bt crystals (~5 vol.%) ranging from 0.75 mm to 2 mm. The poikilitic textures are observed where Pl crystals are enclosed by Hbl. Opaque minerals represent the main accessory phases in these rocks.

Fl-16-11 Qtz-diorite zircon sample contains large euhedral to subhedral crystals and crystal fragments and a few rounded small zircons (most grains are over 500 μm long, Supplementary material). Most of them are stubby crystals (e.g. 2, 3, 9), and only a few smaller acicular grains are present (e.g. 11, 12, 13). Zonation patterns are almost absent in this zircon population, except for the faint concentric zoning observed in the inner area of some grains (e.g. 10) and the apical area of a few crystals (e.g. 7). Th/U ratios are comprised between 0.39 and 0.94 (Table 2).

Eighteen analyses yield $^{206}Pb/^{238}U$ ages between 194 Ma and 185 Ma giving a concordia age of 188.6 ± 2.5 Ma (MSWD = 1.5; Probability = 0.22; Fig. 8d). However, a best fit can be obtained distributing the results in an older set of analyses that yield the same age within analytical uncertainty (MSWD = 0.57; Probability = 0.91), giving a concordia age of 191.4 ± 1.9 Ma (Fig. 8d), and a younger group giving a concordia age of 186.3 ± 1.8 Ma ($N = 9$; MSWD = 0.2; Probability = 0.99) (Fig. 8d). This younger group contains most of the smaller acicular and rounded zircon grains.

5.2.5. Granodiorite FL-16-12

This mesocratic medium-grained rock exhibits two main textural domains. Where igneous textures are present, they present equigranular, hypidiomorphic and phaneritic textures. However, granoblastic textures are dominant over wide areas, where Hbl-Pl-Qtz triple junctions, poikiloblastic Kfs and an extensive recrystallization are observed. The mineralogical composition is dominated by subhedral and twinned Pl (~45 vol.%) with a grain size of

Please cite this article in press as: Rodríguez, N., et al., The significance of U–Pb zircon ages in zoned plutons– the case of the Flamenco pluton, Coastal Range batholith, northern Chile, Geoscience Frontiers (2018), https://doi.org/10.1016/j.gsf.2018.06.003

0.5–1.25 mm that are weakly to moderately altered to sericite, anhedral Qtz (~30 vol.%) ranging from 0.15 mm to 0.5 mm, subhedral Hbl (~10 vol.%) and Bt (~10 vol. %) with crystals smaller than 1.5 mm and subhedral Kfs (~5 vol.%) showing a grain size of 0.25–1.5 mm. Scarce and small opaque crystals represent the main accessory phases in this granodioritic rock.

Medium to small-grained stubby zircons (100–200 μm long and 3:1 to 2:1 aspect ratios) from the sample FL-16-12 are mainly characterized by the presence of external high-luminosity overgrowths that crosscut the former internal zoning patterns of the zircon grains (Fig. 8e). The high-luminosity recrystallization covers the external shape of the crystal and reaches the inner zircon area. The round inner limits of these overgrowths are sharp but vaguely mimic the external shape of the zircon crystals (Fig. 8e, Supplementary material). These recrystallization areas are described in high-grade metamorphic rocks (Corfu et al., 2003). Th/U ratios of these external growths are comprised between 0.46 and 0.67, while the inner zones present more variable values between 0.69 and 1.26 (Fig. 8e, Table 2).

Three Proterozoic and one Ordovician inherited ages were analyzed in the cores of the inner zircon areas. Younger Carboniferous inherited ages were found (329 Ma and 312 Ma). Spots located in the external overgrowths give scattered $^{206}Pb/^{238}U$ ages between 288 Ma and 191 Ma (Fig. 8e, Table 2). The inner undisturbed areas of recrystallized zircons were analyzed resulting a main group that yields the same age within analytical uncertainty (MSWD = 0.002; Probability = 0.97), giving a concordia age of 191.7 ± 1.4 Ma. An older age of 201 ± 5 Ma and a younger simple small crystal that yields a $^{206}Pb/^{238}U$ age of 183 ± 4 Ma complete the age range analyzed in the inner zircon areas (Fig. 8e, Table 2).

5.2.6. Granodiorite FL-16-15

FL-16-15 sample shows fine to medium-grained hypidiomorphic, inequigranular, phaneritic and poikilitic textures. The mineralogical composition is dominated by subhedral and twinned Pl crystals (~40 vol.%) ranging from 0.4 mm to 3 mm that are moderately to strongly altered to sericite. Besides, anhedral >1 mm Qtz (~30 vol.%), subhedral Bt (~20 vol.%), with a grain size of 0.7–3 mm, that are altered to Chl and Ep and anhedral to subhedral 0.25–2 mm Hbl (~10 vol.%) are also present. Poikilitic textures are observed in the smaller crystals Hbl and Qtz that are enclosed by Bt.

Sample FL-16-15 presents euhedral medium-to coarse-grained zircons. They are mostly simple crystals although a few inherited cores can be distinguished. Acicular elongated zircons (over 5:1 aspect ratios) and stubby crystals are contained in this zircon population (Fig. 8f). Most of them show a continuous zonation pattern from the inner to the outer area, although a discontinuous concentric zoning is observed in a few external overgrowths (e.g. zircons 5 and 7, Supplementary material). Th/U ratios are comprised between 0.51 and 1.06, except for analysis 8.1 (Th/U = 1.62) that present the highest U and Th contains (Table 2).

U–Pb zircon ages found in the FL-16-15 sample range of 224 Ma and 183 Ma. This scattering in the geochronological results is due to the presence of a group of older ages between 200 Ma and 224 Ma and a few crystal overgrowths that yield the youngest ages in this sample between 188 Ma and 183 Ma (Fig. 8f, Table 2). Oldest ages are found in the external area of a zircon with inverted ages (younger core than rim) and a simple crystal that give 224 ± 5 Ma and 220 ± 5 Ma respectively. In addition, a large acicular zircon yields a $^{206}Pb/^{238}U$ age of 208 ± 5 Ma. The remaining analyses show an almost continuous age range between 202 and 189 Ma in simple zircons, all of which yield the same age within analytical uncertainty (MSWD = 0.59; Probability = 0.44) giving a concordia age of 194 ± 1.3 Ma (Fig. 8f). The three youngest ages in the FL-16-15 sample are comprised between 188 Ma and 183 Ma analyzed in the apparent younger inner areas of composed zircons (zircons 2, 4, 5) (Table 2, Supplementary material).

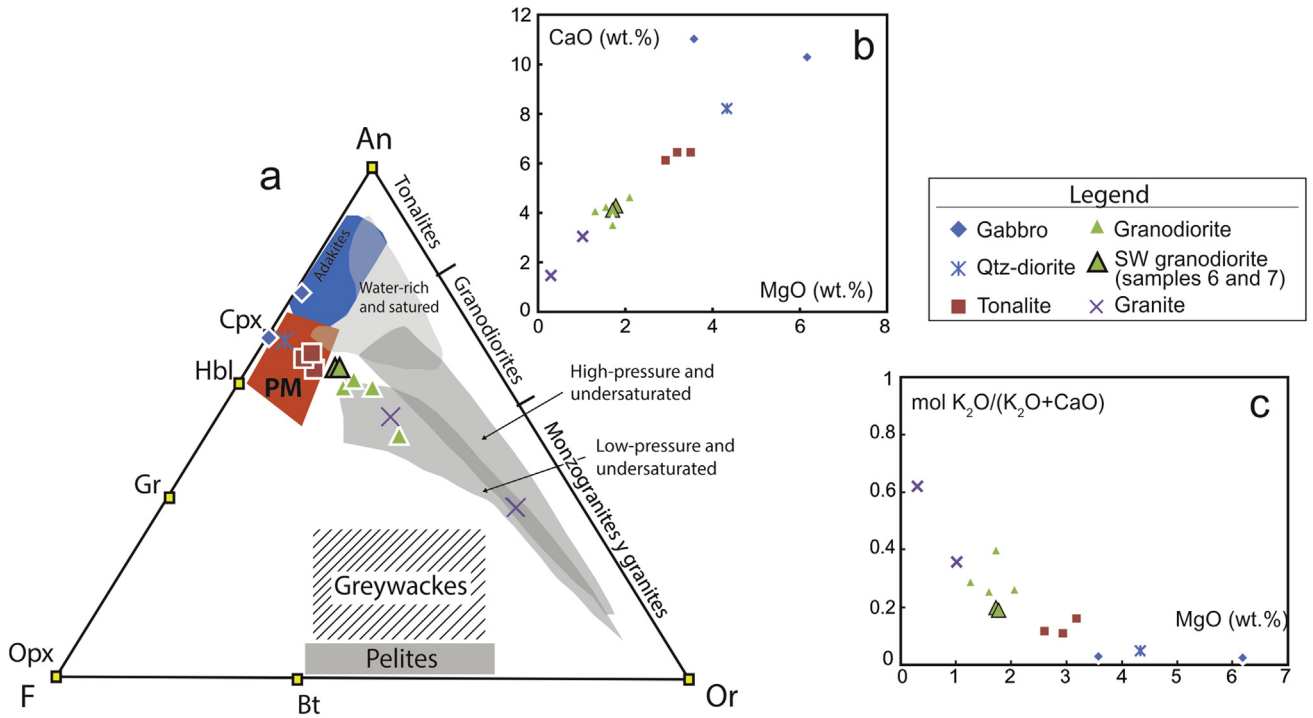

Figure 5. (a) Projected space defined by Opx-An-Or. The main compositional areas and the experimental granitic trends are indicated (Díaz-Alvarado et al., 2011; Castro, 2013 and references therein). (b) and (c) CaO vs. MgO and mol $K_2O/(K_2O + CaO)$ vs. MgO showing the mostly linear trend defined by the Flamenco pluton samples.

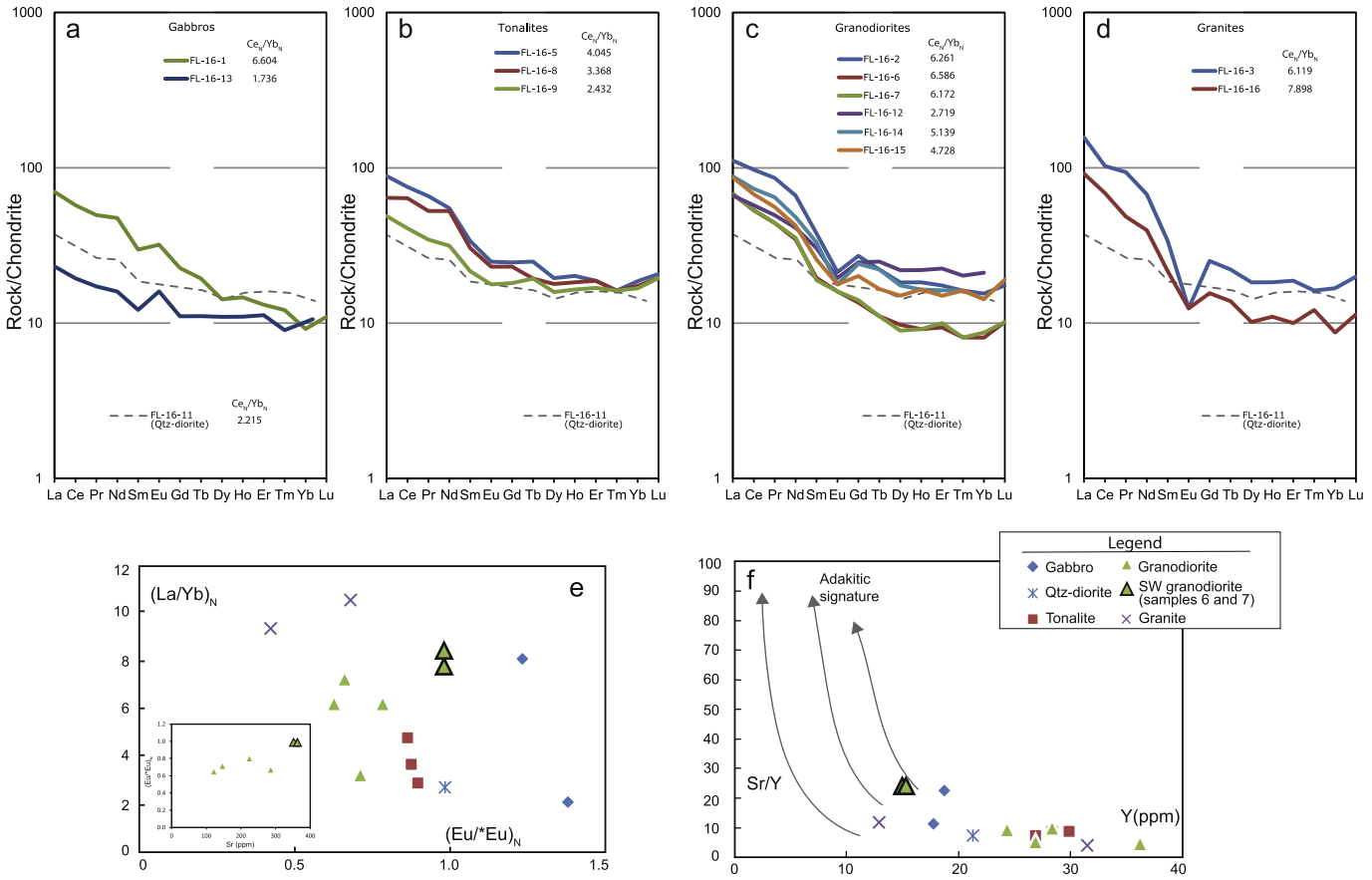

Figure 6. Chondrite-normalized (Nakamura, 1974) REE diagrams for the gabbros and Qtz-diorite (a), tonalites (b), granodiorites (c) and granites (d) of the Flamenco pluton. Ce_N/Yb_N values are indicated as a proxy of the steepening of the REE pattern. (e) $(La/Yb)_N$ vs. $(Eu/*Eu)_N$ diagram showing the higher Eu anomalies, lower $(Eu/*Eu)_N$, in more evolved magmas, except for the FL-16-6 and -7 granodiorites (SW leucocratic granodiorites), where the Eu anomaly is almost absent. The inset shows the highest $(Eu/*Eu)_N$ and Sr values of these samples among the studied granodiorites. (f) Sr/Y vs. Y diagram showing the low Sr/Y values presented by most of the Flamenco samples. The highest Sr/Y values are analyzed in the SW leucocratic granodiorites.

5.2.7. *Porphyritic dike ME-16-2*

The tonalitic dike was sampled 8 km to the north of the Flamenco pluton. It consists of euhedral to subhedral Hbl and Pl crystals included in a highly altered microcrystalline matrix. The porphyritic dike contains mostly medium-to small-grained simple stubby zircons. The largest crystals (250 μm long) are simple acicular zircons with parallel-banded zonation (e.g. zircon 12, Supplementary material). However, the most abundant zircons are 100–150 μm stubby crystals with pyramidal tips and oscillatory concentric zoning. One compositionally zoned zircon with an inherited core was found (zircon 10, Supplementary material). Th/U ratios are between 0.58 and 0.32 (Table 2).

One Tonian age (783 ± 11 Ma) was analyzed in an inherited core. The remaining fifteen analyses yield $^{206}Pb/^{238}U$ ages between 214 Ma and 191 Ma. The main group (202–191 Ma) gives the same age within analytical uncertainty (MSWD = 0.36; Probability = 0.55), giving a concordia age of 197 ± 2.2 Ma (Fig. 8g). A simple zircon yielded the oldest age of 214 ± 4 Ma (Fig. 8g, Table 2).

5.2.8. *Host metasediments FL-16-4*

The metasediments (Las Tórtolas Formation) that host the intrusive magmas were sampled in the southern contact of the Flamenco pluton (Fig. 1c), where the metamorphic aureole is more extensively developed (Rodríguez et al., 2016). Fine- to medium-grained Crd-schists consist of metagraywackes interbedded with quartzites. The mineral assemblage consists of rounded Qtz crystals, subhedral grains of Kfs, subhedral Pl grains, subhedral grains of Bt and a groundmass of altered Crd. Where cordierite subhedral grains are distinguished, they show abundant, small, drop-like inclusions of Qtz and small flakes of Bt.

Sample FL-16-4 mostly contains 100–250 μm long anhedral rounded zircons and zircon fragments. Only a few of them present a CL-dark external prismatic overgrowth (e.g. zircons 3, 7 and 13) (Fig. 8h). Simple rounded zircons, inherited cores and most overgrowths give Th/U ratios between 0.11 and 0.60. The three youngest

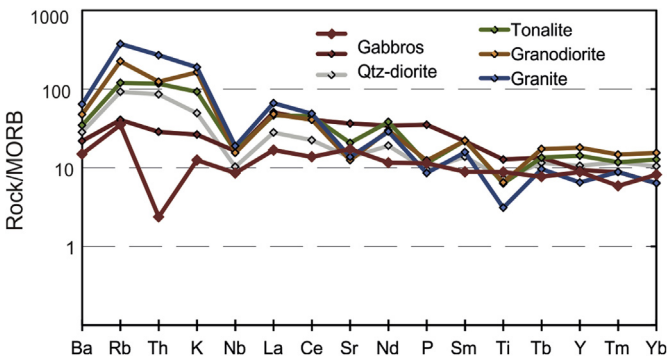

Figure 7. Thompson normalization plot rock/MORB for representative samples of the Flamenco intrusives.

Please cite this article in press as: Rodríguez, N., et al., The significance of U–Pb zircon ages in zoned plutons– the case of the Flamenco pluton, Coastal Range batholith, northern Chile, Geoscience Frontiers (2018), https://doi.org/10.1016/j.gsf.2018.06.003

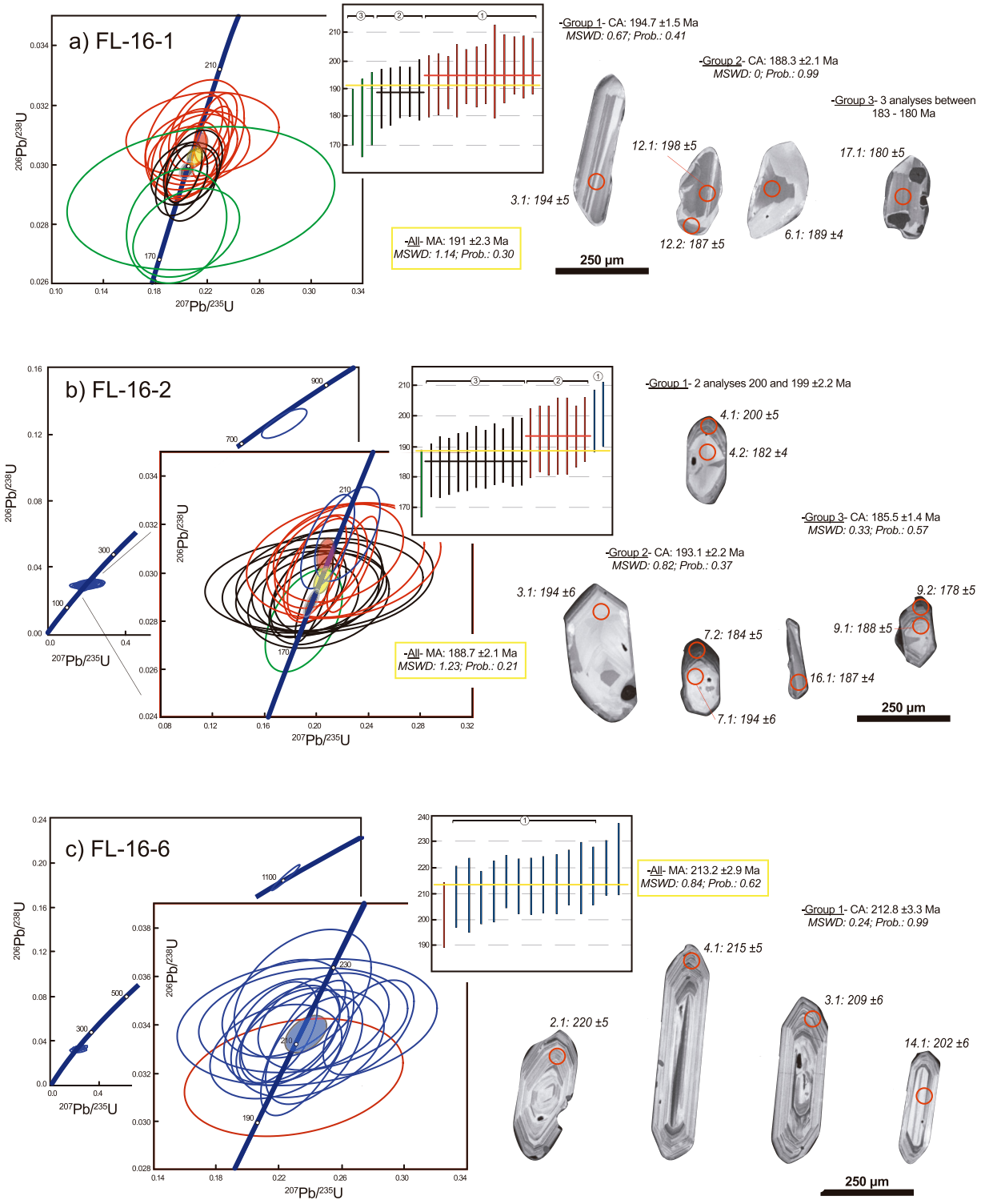

Figure 8. U–Pb Concordia and error-bar (2σ) diagrams of the studied samples. Error ellipses and bars show distinct colors for each group of zircons exhibiting specific morphological features or distinctive ages (see text for details). CL images of representative zircons of the studied samples are included (see Supplementary Material to study the zircon populations and analyzed crystals for each sample). Mean $^{206}Pb/^{238}U$ ages for all analyzed data and for selected groups are indicated. Error ellipses in Concordia diagrams represent a 68.3% conf., including the standard error. (a) FL-16-1 gabbro. (b) FL-16-2 granodiorite (c) FL-16-6 granodiorite. (d) FL-16-11 Qtz-diorite. (e) FL-16-12 granodiorite. The inset show the different Th and U values measured in external overgrowths and inner areas of the zircons (f) FL-16-15 granodiorite. (g) ME-16-2 porphyritic dike. (h) FL-16-4 metasediment. A relative probability histogram is presented for this sample to show the main ages registered in the host metasediments.

Please cite this article in press as: Rodríguez, N., et al., The significance of U–Pb zircon ages in zoned plutons– the case of the Flamenco pluton, Coastal Range batholith, northern Chile, Geoscience Frontiers (2018), https://doi.org/10.1016/j.gsf.2018.06.003

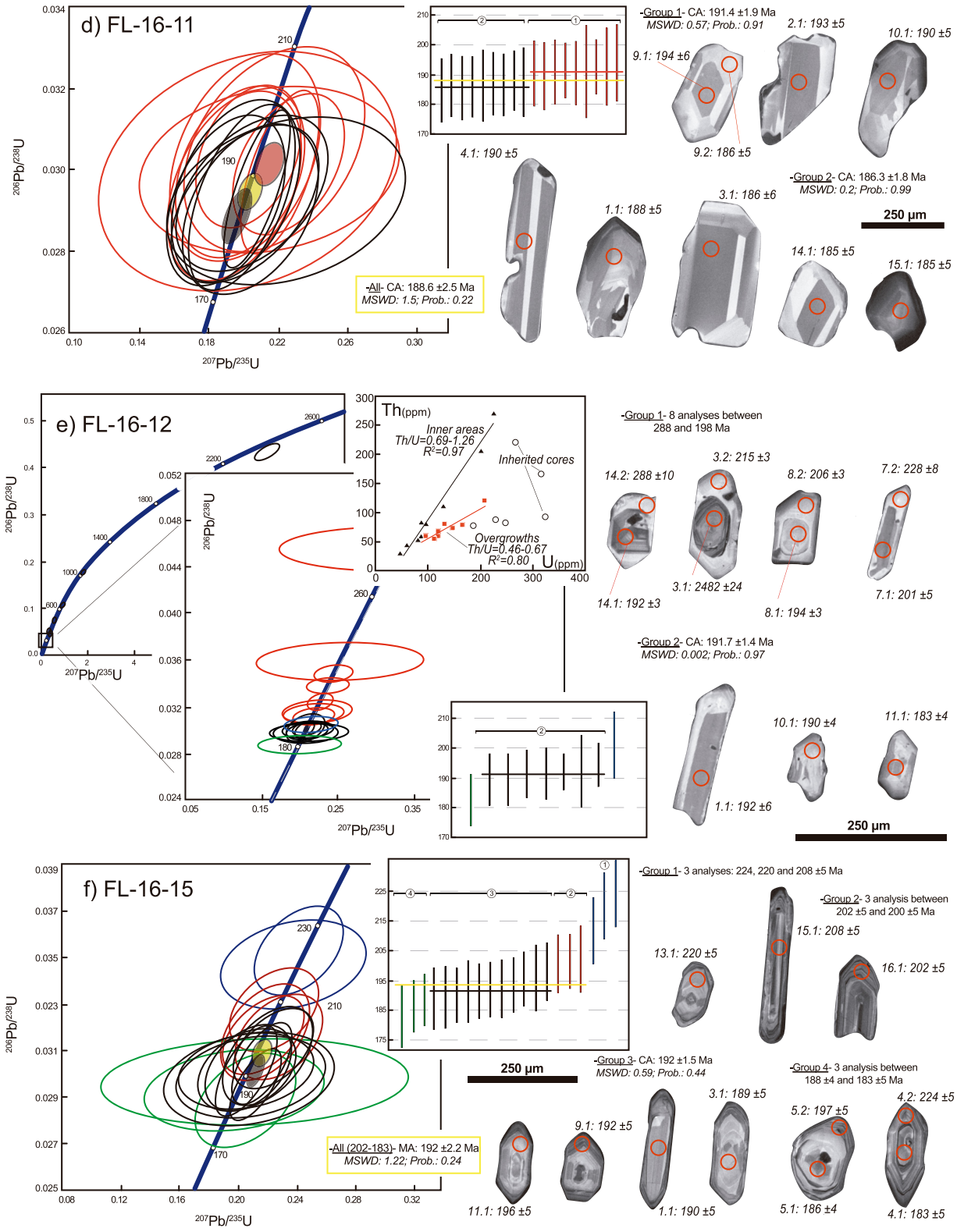

Figure 8. (*continued*).

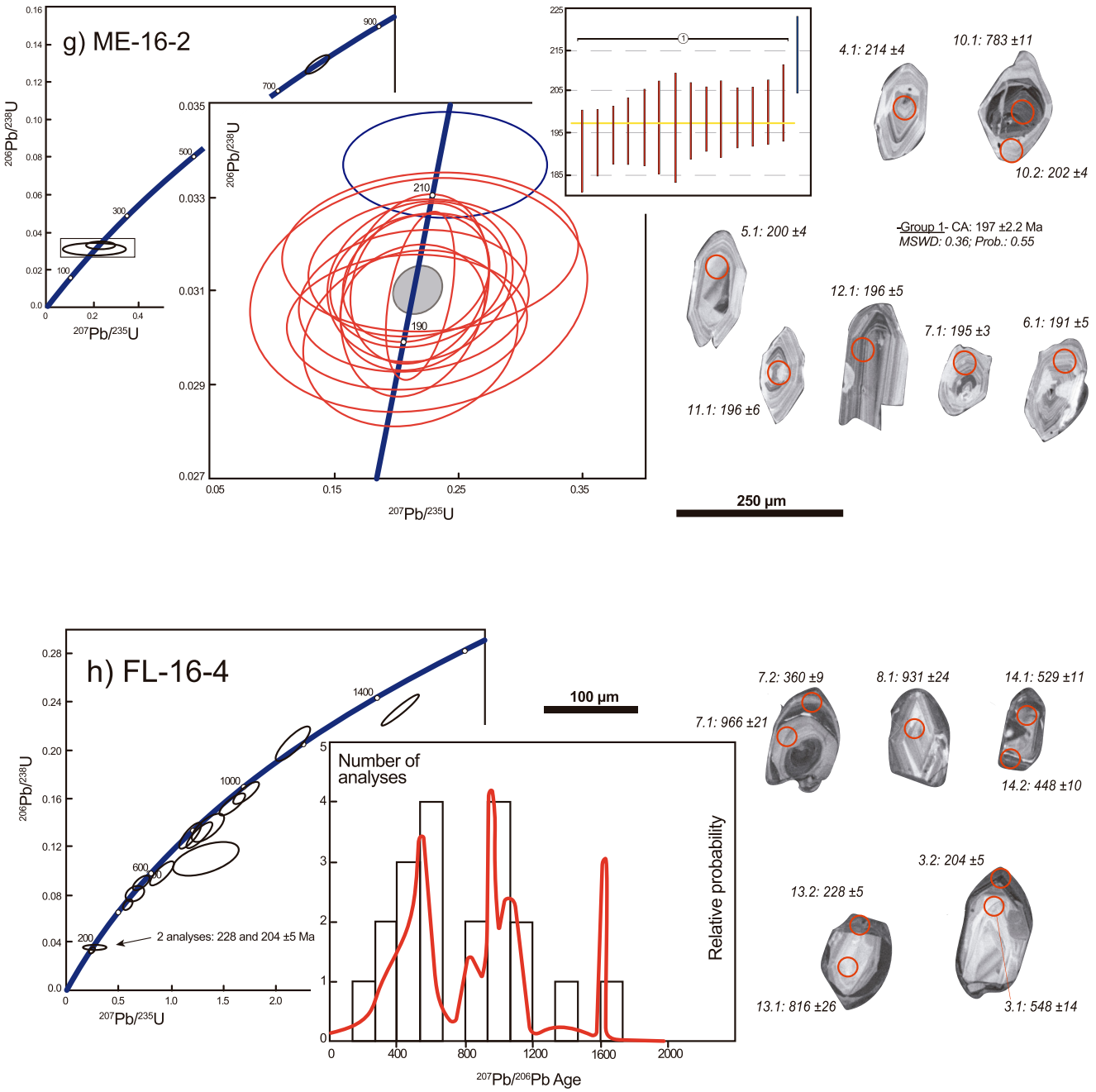

Figure 8. (*continued*).

ages analyzed yield the lowest Th/U ratios of 0.1 and 0.02, which are related to metamorphic overgrowths and felsic per aluminous melts (e.g. Williams, 2001; Wang et al., 2011).

Inherited ages of the metasedimentary rocks include two Mesoproterozoic, six Tonian, one Cryogenian, seven upper Neoproterozoic-Cambrian and one Upper Ordovician ages (Fig. 8h, Table 2). Younger ages were analyzed at the tips of three zircons where the external overgrowths were wide enough to locate the spot. A $^{206}Pb/^{238}U$ age of 360 ± 9 Ma and two Upper Triassic ages (228 ± 5 and 204 ± 5 Ma) were obtained in these low Th/U metamorphic overgrowths, being these results related with the older ages described in the granitic rocks of the Flamenco pluton (Fig. 8).

6. Discussion

6.1. U–Pb zircon geochronology perspectives on the emplacement process of the Flamenco pluton

6.1.1. The statistical approach to the U–Pb zircon ages, the gestation of unmeaning geological ages?

The use of geochronological data either as single ages or as a group of ages that, representing the same event, are approximated by statistics is still controversial (Spencer et al., 2016). Experts on the analytical process of the SIMS geochronology mostly agree that the sources of imprecision and inaccuracy derive from the

analytical techniques, the sample and instrument-related uncertainties, i.e., counting statistics, sample heterogeneity and instrument issues: chamber pressure, sample surface charging and temperature, primary beam intensity or spot shape drift (Compston, 2001; Black and Jagodzinski, 2003; Jeon and Whitehouse, 2014). The employment of rigorous analytical protocols and the accuracy of the standards used to correct former data can minimise but not eliminate the errors inherent to the analytical technique (Jeon and Whitehouse, 2014).

Assessing the analytical uncertainties and the paradoxical fact that wide ranges of ages, larger than expected for SIMS techniques, are obtained from a few kilograms sample lead to the use of statistics and mean ages. The statistical mean is a vulnerable parameter to extreme data, considering only more central or recurrent values, but rejecting oldest, youngest or less numerous analyses. These data frequently show confidence parameters as common Pb, the standard deviation of the $^{206}Pb/^{238}U$ ratios or the discordance percentage indistinguishable from those of the data included in the average. The latter parameters do not completely guarantee the similarity between the result derived from the U–Pb ratios and the real age. However, if we consider that the error estimates include all the methodological uncertainties, we take into account zircon morphology and internal structure and we argue other available geological evidences as field relations and geochemistry, geochronological data (including individual and mean ages) obtained from SIMS geochronology are reliable and meaningful to depict complex geological processes (e.g. Rubatto, 2002; Coleman et al., 2004; Miller et al., 2007, 2011; Díaz-Alvarado et al., 2013; Pereira et al., 2014, 2015; Fiannacca et al., 2017).

The studied samples of the zoned Flamenco pluton include gabbros, Qtz-diorites, tonalites and granodiorites (Figs. 1,3), in addition to a sample from a tonalitic dike, located 8 Km to the north of the pluton, thought still related to the emplacement process (Fig. 8), and the host metasediments from the southern contact aureole. A set of data of 16 to 23 analyses was obtained for each sample. Measured ^{204}Pb was preferred to correct the common Pb. The $^{206}Pb/^{238}U$ ages were used as geochronological reliable results, with error values (1σ) between ± 4 and ± 8 for Upper Triassic and Jurassic ages, while the error percentages for $^{206}Pb/^{238}U$ ratios resulted between 1.6 and 3.8 (Table 2). The geochronological results show $^{206}Pb/^{238}U$ intra-sample age differences between 9 Myr and 41 Myr (Fig. 8, Table 2) for non-inherited ages. The narrowest age ranges resulted from unzoned zircons from the FL-16-11 Qtz-diorites, between 194 Ma and 185 Ma (Fig. 8d, Table 2), and the tonalitic dike ME-16-2 between 202 Ma and 191 Ma, without considering an oldest $^{206}Pb/^{238}U$ age of 214 ± 5 Ma (Fig. 8g, Table 2). Wider age ranges were found in the magmatic facies that apparently show larger volumes to the NW and SE of the Flamenco pluton: FL-16-2 tonalite (Fig. 8b, Table 2) gives ages between 200 Ma and 178 Ma, and FL-16-15 granodiorite (Fig. 8f, Table 2) yields a $^{206}Pb/^{238}U$ age range of 41 Myr, between 224 Ma and 183 Ma.

The distribution of the results throughout the $^{206}Pb/^{238}U$ age ranges is similar in most of the Flamenco pluton samples and resembles the results obtained in several studies that use the same methodology in granitic rocks (e.g. Jeon et al., 2012; Díaz-Alvarado et al., 2013; McKay et al., 2015; Pereira et al., 2014, 2015; Fiannacca et al., 2017). The dataset comprises a few analyses that give older ages and are significantly separated from the main group (differences are larger than the $\pm$ interval). These analyses (blue bars and ellipses, Fig. 8) yield $^{206}Pb/^{238}U$ ages between 200 Ma and 225 Ma and are only absent in samples FL-16-1 and -11 (gabbros and Qtz-diorites). A few $^{206}Pb/^{238}U$ ages between 188 Ma and 178 Ma (202 Ma in sample FL-16-6, Fig. 8c) are scattered with younger results than the main groups (green bars and ellipses, Fig. 8). Some of these extreme results (oldest and youngest ages) were obtained from complex zircons that present a young core rounded by an older overgrowth (zircons 2 and 4 in sample FL-16-15 and zircon 4 in sample FL-16-2). These results may reflect the disturbance of radiogenic isotopes, with the younger age indicating radiogenic Pb loss, or standard correction problems. However, the same ages are also present in simple and "normally" (older core than rims) zoned zircons (zircon 13 in sample FL-16-15 and zircon 5 in sample FL-16-2). Moreover, the oldest ages are not randomly distributed between 200 Ma and 225 Ma, by contrast they are grouped around 200 Ma, 213 Ma and 220 Ma despite the geochemical and geochronological differences described between the Flamenco pluton samples, including the oldest FL-16-6 granodiorite and the dike (ME-16-2). Meaningfully, similar ages were obtained from the scarce and narrow metamorphic overgrowths analyzed in zircons from the host metasediments (204 ± 5 Ma and 228 ± 5 Ma, Fig. 8h).

The larger set of analyses, grouped between 198 Ma and 186 Ma (within the $\pm$ interval), give concordia and weighted mean ages between 197 Ma and 188 Ma, except for oldest FL-16-6 sample. Statistically, these ages present low probabilities and MSWD >1 for most samples due to the scattering of these results. If we consider smaller subgroups, it is evident that the statistical results will be improved (Fig. 8). Nevertheless, these subgroups are representative when they include the analyses of morphologically similar zircons or zircon zones, e.g. FL-16-2 and -11 (Fig. 6, Table 2). A useful statistical approach to unravel the composition of a U–Pb zircon data population is the reduced chi-squared statistic (X^2_{red}), also known as the MSWD (Wendt and Carl, 1991; Spencer et al., 2016). If we plot the 1σ MSWD values vs. the number of analyses for the samples FL-16-1, -2, -11 and -15, the statistical results derived from the mean ages of all data and subgroups are clearly separated (Fig. 9). Although most of these X^2_{red} values are included in the acceptable field, if we consider all data, the MSWD values between 1.15 and 1.5 may represent a composite population. On the other hand, the MSWD values resulted from the subgroups are in the range of 0.2–0.82 (and an extremely low MSWD value for a smaller subgroup in the FL-16-1 sample) (Fig. 9), which suggest that the uncertainties of the mean ages of these subgroups may be overestimated (Spencer et al., 2016). The confidence of these results may be called into question due to the amount of data although most of the geochronological studies cited here present between 15 and 30 analyses per sample. Even accounting for this geochronological results distribution, it must be considered the overlapping of individual and group ages (including errors) resulted in most Flamenco pluton samples (Fig. 8).

Sample FL-16-12 shows an outstanding example of complex zircons. A significant amount of zircons show high luminosity rims that grow from the external area of the crystal crosscutting the former zonation, preserved in the irregular rounded inner area of the zircon (Fig. 8e). Similar zoning patterns have been described in zircons from high-grade metamorphic rocks (Corfu et al., 2003). Further, these overgrowths are observed in zircons from tonalitic rocks where granulitic textures have been described (Fig. 2b) (Rodríguez et al., 2016). Geochronological results obtained from the analysis of these overgrowths yield $^{206}Pb/^{238}U$ ages between 198 Ma and 288 Ma, although a few younger small-grained crystals may be affected by this recrystallization process. These ages are not related to instrument-related uncertainties but may be the result of diffusion processes that resulted in the variation of isotopic ratios. The metamorphic process would promote the scattering of the $^{206}Pb/^{238}U$ ages and the variation of Th/U ratios (Fig. 8e, Table 2). The effects related to the Pb diffusion in pre-magmatic zircons have been studied through 3D numerical models (Bea and Montero, 2013), and may be considered for antecrysts and autocrysts (Miller et al., 2007, 2011) in magmatic sequential emplacement and

Please cite this article in press as: Rodríguez, N., et al., The significance of U–Pb zircon ages in zoned plutons– the case of the Flamenco pluton, Coastal Range batholith, northern Chile, Geoscience Frontiers (2018), https://doi.org/10.1016/j.gsf.2018.06.003

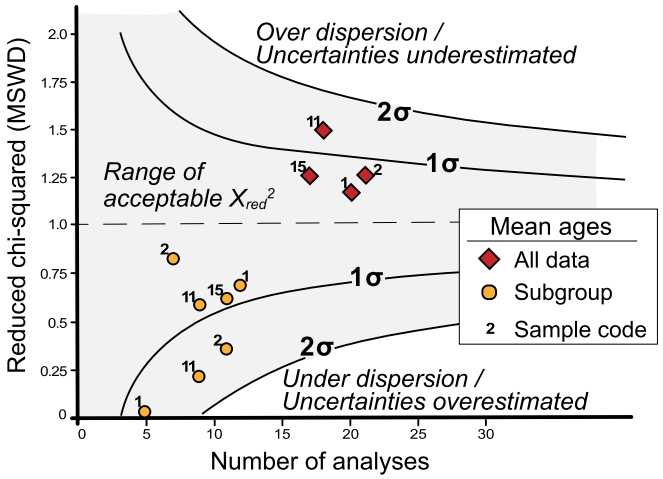

Figure 9. Reduced chi-squared (MSWD) vs. the number of analyses for the samples FL-16-1, -2, -11 and -15 showing the differences in the statistical values if we consider all data or the significative subgroups. MSWD and probability values of these mean ages can be consulted in Figs. 8 and 11. Modified from Spencer et al. (2016).

rejuvenation processes. According to the models, the magnitude of the diffusion mostly depends on the temperature of the new magma batch and the presence of zircons as inclusions or as free crystals, and diffusion promotes the Pb migration from U-rich to U-poor zircon domains (Bea and Montero, 2013). In the FL-16-12 sample, recrystallization affected the crystal margins, likely under sub-solidus conditions. However, in the case of antecrysts that are entrained in new magma batches, the diffusion of radiogenic isotopes must be taken into account for the entire volume of the crystal (Cherniak, 2010; Bea and Montero, 2013).

The Th/U ratios of zircons may also distinguish geologically significative groups of ages and geochemical changes in the zircon-forming crystallization environment (Williams, 2001; Wang et al., 2011; Pereira et al., 2014). The Th content, which shows a lower distribution coefficient (Kd) than U in zircon, is related to the higher crystallization temperatures of mafic magmas, evidencing different physical and chemical conditions during crystallization (Wang et al., 2011; McKay et al., 2018). Indeed, the zircons from the FL-16-1 gabbros show the highest Th/U ratios (Fig. 10), while the lowest ratios are observed in the zircon overgrowths from the host metasediments (Th/U < 0.1). The Th/U averages obtained in the Flamenco pluton samples range from 0.67 to 0.87. Although there

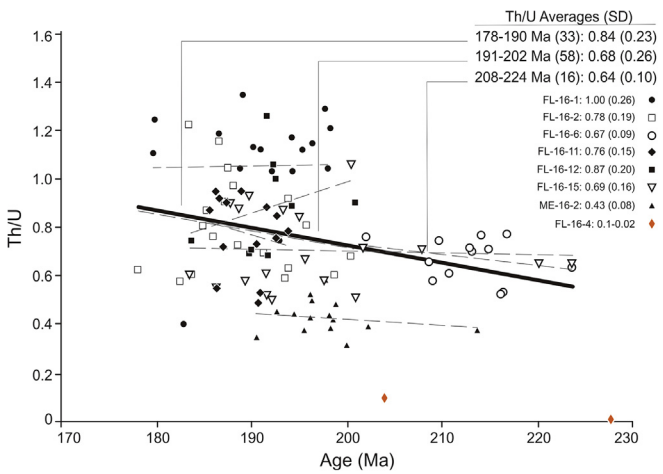

Figure 10. Variation of the Th/U ratios with time. Solid and dashed lines represent the trend line for all and each sample respectively.

are cores and rims of the same age with different Th/U ratios, in general, younger samples have higher Th/U ratios (Fig. 10). If we consider the results of all granitic samples, the analyses that yield $^{206}Pb/^{238}U$ ages between 191 Ma and 202 Ma have a Th/U ratio average of 0.68, while the analyses with ages between 190 Ma and 178 Ma show a Th/U average of 0.84. Even though these results present broad trends, Th/U ratios indicate variations in the chemical conditions of the melt that may explain the differences in the cores and rims of complex zircons that crystallized during the interaction between different magma batches in zoned plutons (Miller and Wooden, 1994; Wang et al., 2011; Pereira et al., 2014, 2015).

6.1.2. Building of the zoned Flamenco pluton through the sequential emplacement of magma batches

The geochronological results obtained from the magmatic facies that comprise the Flamenco pluton show a wide range of ages in most samples and point to an extended zircon crystallization process between 220 Ma and 180 Ma (Fig. 11). However, significant sets of analyses are grouped and could be interpreted as major zircon crystallization events. These crystallization ages are related to the emplacement process of the pluton, which shows shorter or longer duration according to volumes and temperatures of magma batches and the timing of replenishment and rejuvenation processes (e.g. Huber et al., 2010, 2011; Burgisser and Bergantz, 2011; de Saint Blanquat et al., 2011; Miller et al., 2011; Paterson et al., 2011; Díaz-Alvarado et al., 2013). As many of these highlighted groups of ages and calculated errors overlap, we rely on other evidences described in this study to assess the geological meaning of geochronological results.

The first emplaced magmatic facies among the studied samples is the FL-16-6 granodiorite between 220 Ma and 210 Ma, with a best estimate for the crystallization age of 212.8 ± 3.3 Ma (N = 12, MSWD = 0.24, Prob. = 0.99) (Fig. 11). This sample represents the leucocratic granodiorites located at the SW area of the Flamenco pluton (FL-16-6 and -7, Fig. 1c), which show some distinguishable geochemical characteristics as the absence of the Eu anomaly, a distinctive depletion in HREE and high Sr contents (Fig. 6). Except the tonalitic dike, with a best estimated crystallization age of 197 ± 2.2 Ma (N = 14, MSWD = 0.36, Prob. = 0.55), the rest of the studied samples in the Flamenco pluton present a major group of $^{206}Pb/^{238}U$ ages between 196 Ma and 186 Ma. The mean ages calculated for these samples yield 188.7 ± 2.1 Ma and 188.6 ± 2.5 Ma for FL16-2 and -11 samples and 191 ± 2.3 Ma, 191.7 ± 1.4 Ma and 192 ± 2.2 Ma for FL16-1, 12 and 15 samples respectively. However, according to the results reported above, including the statistical approach (Fig. 9), a more accurated description of the emplacement sequence may be achieved.

To the NW, FL-16-12 and FL-16-15 granodiorites represent the inner area of the pluton with respect to the mafic external area comprised by gabbros and Qtz-diorites (FL-16-11) (Fig. 1c). Inner magmatic facies show subgroups of ages analyzed in simple zircons and the inner area of complex zircons that give nearly identical concordia ages of 191.7 ± 1.4 Ma (N = 8, MSWD = 0.002, Prob. = 0.97) for the FL-16-12 sample and 192 ± 1.5 Ma (N = 11, MSWD = 0.59, Prob. = 0.44) for the FL-16-15 sample. For the external FL-16-11 Qtz-diorites, simple unzoned zircons present two significative set of ages. The first group yields an age of 191.4 ± 1.9 Ma (N = 9, MSWD = 0.57, Prob. = 0.91) that is also identical within error to the samples collected in the inner area of the Flamenco pluton. A second group gives an age of 186.3 ± 1.8 Ma (N = 9, MSWD = 0.2, Prob. = 0.99), which likely represents the younger crystallization age of the external magmatic batches. We suggest that the later emplacement of the mafic magmas at the external area of the Flamenco pluton triggered the granoblastic

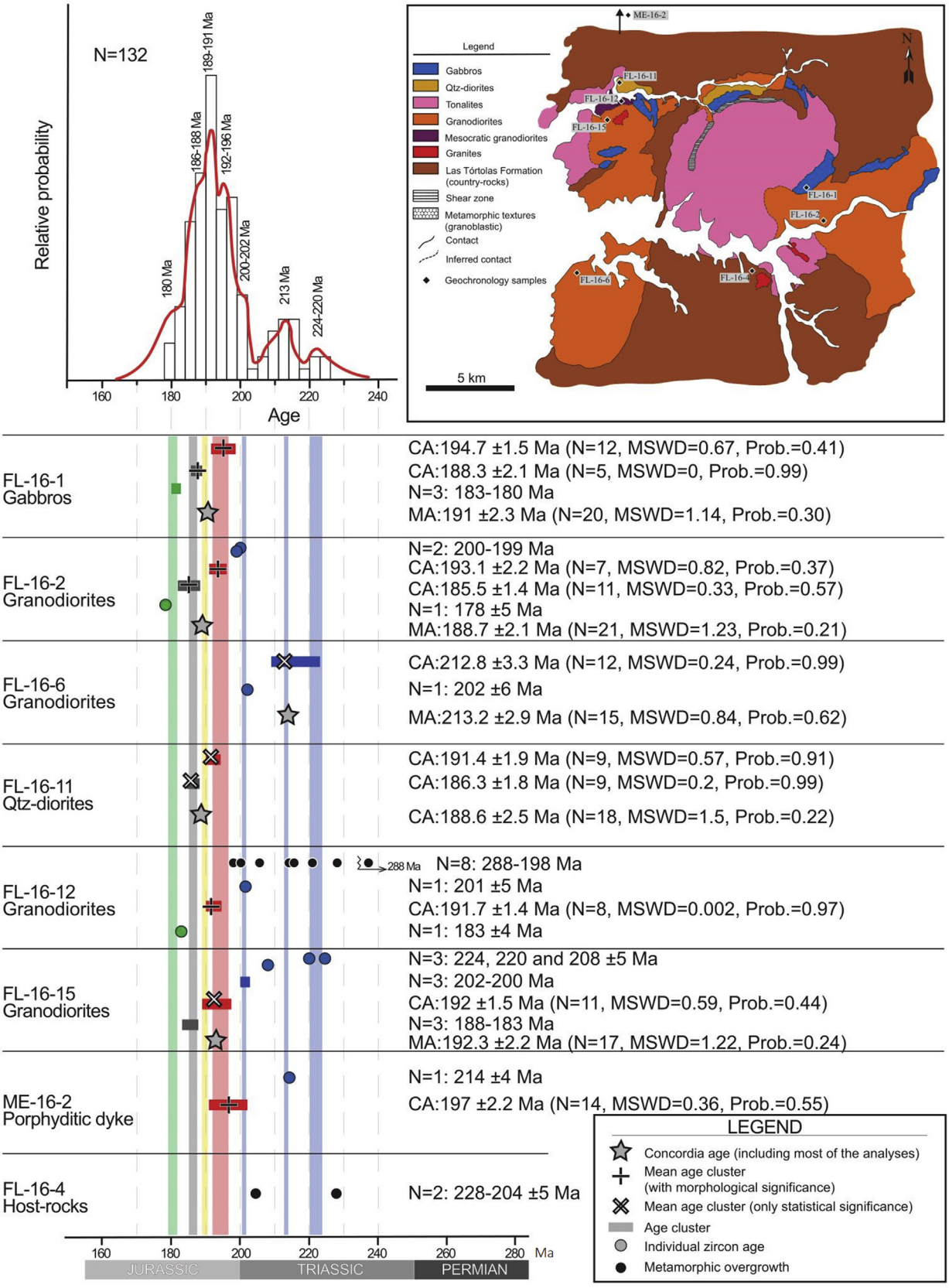

Figure 11. Schematic U–Pb zircon age diagram for the Flamenco pluton samples. The vertical bars relate the major age peaks of the histogram with the mean and concordia ages calculated for each sample, and allow to define chronological links between samples and age clusters. The exact ages and errors represented by the symbols can be consulted in the main text, Fig. 8 and the right side of the scheme. Bar colors are referred to the error ellipses and bars of Fig. 8. The figure includes a schematic geological map of the pluton after the geochemical and the geochronological study.

Please cite this article in press as: Rodríguez, N., et al., The significance of U–Pb zircon ages in zoned plutons– the case of the Flamenco pluton, Coastal Range batholith, northern Chile, Geoscience Frontiers (2018), https://doi.org/10.1016/j.gsf.2018.06.003

recrystallization observed in the FL-16-12 granodiorites (Fig. 2b). This process is revealed in the high-temperature overgrowths observed in the zircon crystals and the disturbance of isotopic and Th/U ratios in these recrystallized areas (Figs. 8e and 11, Table 2). These mesocratic granodiorites comprise the border facies of the granodiorites that dominate the inner area of the Flamenco pluton in its NW area. The transitional contacts, the geochemical characteristics and the coincident crystallization ages suggest an in-situ normal differentiation process from granodiorites (FL16-12 and -15) to the inner granitic facies (FL16-16) (Figs. 1c and 11). On the contrary, the sharp contacts observed between gabbros and Qtz-diorites and the inner felsic magmatic facies, together with the younger crystallization ages of the Qtz-diorites, point to the later external emplacement of mafic magma batches.

To the SE area of the pluton (Fig. 1c), gabbros (FL-16-1) and granodiorites (FL-16-2) present more intricate relations. Two sets of analyses were identified according to the data distribution and the morphological characteristics of zircons. Most of the large euhedral crystals and the inner areas of subhedral complex zircons in the gabbroic sample give a concordia age of 194.7 ± 1.5 Ma (N = 12, MSWD = 0.67, Prob. = 0.41), which agrees within analytical uncertainty with the concordia age of the inner area of large zircons from the FL-16-2 granodiorites, i.e. 193.1 ± 2.2 Ma (N = 7, MSWD = 0.82, Prob. = 0.37). A major group of morphologically diverse zircons in FL-16-2 yield a concordia age of 185.5 ± 1.4 Ma (N = 11, MSWD = 0.33, Prob. = 0.57), slightly younger than the age of a few zircon and crystal overgrowths in FL-16-1 gabbros that give a concordia age of 188.3 ± 2.1 Ma (N = 5, MSWD = 0, Prob. = 0.99). These ages agree within analytical uncertainty of the crystallization ages described in the NW area of the pluton. Both magmatic facies show a similar age distribution and mean ages, which suggests a simultaneous emplacement process, although the larger number of analyses and the younger concordia age resulted in the latter group of the FL-16-2 sample (185.5 ± 1.4 Ma) may be indicative of a protracted emplacement process for the granodioritic-tonalitic magmas that comprise most of the eastern domain of the pluton. This is in agreement with the magma-magma relations observed in this area of the pluton and the sub-solidus textures developed in the firstly crystallized gabbroic magmas (Fig. 2c,d).

Despite the identical (within error) zircon crystallization ages, the NW and E areas of the Flamenco pluton show dissimilar emplacement processes according to the observed field relations, which are in agreement with the zircon ages and characteristics described above. In the NW plutonic area, the emplacement sequence agrees with low replenishment rates. Therefore, the older magmatic batches were already crystallized when the younger mafic magmas arrived to the emplacement level, which forced the external location of these pulses and promoted the granoblastic recrystallization of the contact zone of the inner granodioritic facies. To the E of the Flamenco pluton, intermediate and mafic batches coincided as magmas at the emplacement level. These may be indicative of a higher rate of magma supply. Regardless of these differences, mafic pulses (gabbros and Qtz-diorites) intruded the earlier and more voluminous intermediate magmas. This is in agreement with the higher Th/U ratios found in the younger analyses (Fig. 10) and may be interpreted as a later mafic input in the magmatic source and emplacement regions, which was in equilibrium with the younger zircon crystals.

Granodioritic samples, including the porphyritic dike, contain simple zircons (e.g. 13.1 and 15.1 in FL-16-15 sample, Fig. 8f; 4.1 in ME-16-2 sample, Fig. 8g) as well as complex zircons (e.g. 4 in FL-16-2 sample, Fig. 8b; 4 in FL16-15 sample, Fig. 8f) that yield $^{206}Pb/^{238}U$ ages pooled around specific zircon crystallization events at 200–202 Ma, 213 Ma and 220–224 Ma (Fig. 11). The coincidence of these results in geochronological and geochemically different samples of the Flamenco pluton discards an analytical error. Further, the rare metamorphic rims found in the zircons from the host metasediments at the contact aureole give similar ages (Figs. 8h and 11), suggesting that the crystallization events depicted at 200 Ma and 220 Ma are related to the arrival of magma batches to the emplacement level, as an age of 212.8 ± 3.3 Ma has been proposed for the emplacement of SW granodiorites (FL-16-6). According to the estimates about the cooling rates of magma bodies in the middle to upper crust (e.g. Petford et al., 2000; Paterson et al., 2011), it is improbable that intrusive sheets remain as partially melted magmas during extended periods of 20 Myr. Therefore, these older zircons may provide evidence for processes located at the source or deep storage levels, as partial melting, magma segregation or emplacement. These zircons were likely incorporated as antecrysts to the younger zircon populations that ultimately represent a mixture of antecrysts, restitic crystals, xenocrysts and mainly autocrysts (e.g. Charlier et al., 2005; Miller et al., 2007).

The youngest $^{206}Pb/^{238}U$ ages included in most samples are closer than antecrysts to the assigned crystallization age of the main groups and do not show age agreement between samples, e.g. 178 ± 5 Ma in FL-16-2, 202 ± 6 Ma in FL-16-6 or 183–188 Ma in FL-16-15 (Fig. 11). In FL-16-15 sample, these ages are analyzed in cores that yield younger ages than the rims, while in the rest of samples they are mostly analyzed in small simple crystals (Fig. 8). Accordingly, these slightly younger results may be promoted by late Pb loss, the migration of isotopes under sub- or super-solidus conditions, or date the last stages of the residual melt crystallization.

In summary, wider age ranges are observed in magmatic facies with the largest apparent volumes (samples FL-16-2 and -15) and therefore, the magnitude of these age differences in each sample may be related to the emplacement duration and volume (construction rate) of each magma batch. On the contrary, smaller age ranges obtained in the tonalitic dike and the Qtz-diorites indicate faster crystallization and cooling rates. The same relation has been described at the scale of continental magmatic arcs (de Saint Blanquat et al., 2011). The Flamenco pluton, with an estimated area of 350–400 km^2, is comprised of at least three magmatic domains separated by metasedimentary septa. Although the SW granodioritic domain is significantly older (213.2 ± 2.9 Ma), the NW domain is emplaced between 192 ± 1.5 Ma and 186.3 ± 1.8 Ma while the eastern domain is emplaced between 194.7 ± 1.5 Ma and 185.5 ± 1.4 Ma. Estimations of the crustal structure of the northern Chilean Coastal Range batholith (Grocott and Taylor, 2002) propose 1–2 km thick intrusive layers. Disregarding any syn- and post-emplacement contractional deformation, the total volume of the Flamenco pluton may be estimated between 500 km^3 and 1000 km^3. These volumes and time span of the emplacement process relate this intrusive body to a relevant group of plutons located at convergent settings with construction rates between 0.001 km^3/yr and 0.0001 km^3/yr (de Saint Blanquat et al., 2011).

6.2. Nature of the magmatic source from the observed geochemical and geochronological variations

The Flamenco pluton belongs to the westernmost intrusives alignment of the Coastal Range batholith in northern Chile (Fig. 1). These are considered the first emplaced magmas during the building of the magmatic arc during the inception of the Andean cycle. The magmatic arc axis then migrated progressively to the east, without major interruptions until the late Lower Cretaceous (e.g. Charrier et al., 2007). According to the geochronological results, the Flamenco pluton is comprised by two main magmatic pulses: the leucocratic granodiorites to the SW that yield a best

Please cite this article in press as: Rodríguez, N., et al., The significance of U–Pb zircon ages in zoned plutons– the case of the Flamenco pluton, Coastal Range batholith, northern Chile, Geoscience Frontiers (2018), https://doi.org/10.1016/j.gsf.2018.06.003

estimated crystallization age of 213 Ma, and the gabbros, Qtz-diorites, tonalites and granodiorites that compose most of the intrusive complex, whose U–Pb zircon ages define a sequential emplacement between 194 Ma and 186 Ma (Fig. 11). The limited geochemical differences between the older and younger magma batches involve a long-lasting homogenous and stable magmatic source during the First Stage of the Andean Cycle, as it is characteristic of the Cordilleran-type batholiths along the active convergent margins (e.g. Pankhurst et al., 1999; Parada et al., 1999; Grove et al., 2005; Wagner et al., 2005; Hervé et al., 2007; Castro, 2013). However, there are subtle differences that deserve to be considered. The SW leucocratic granodiorites show higher CaO and Sr contents than the rest of the granodiorites studied in the Flamenco pluton. This older granodioritic pulse, represented by the FL-16-6 and FL-16-7 samples, records Eu/Eu* ratios around the unity (Fig. 6, Table 1). According to the REE contents, the SW granodiorites are depleted in ΣREE and present steep REE patterns due to a major depletion in HREE (Fig. 6c). If we compare these results with laboratory experiments that analyze the phase relations in the metasediment-MORB mélanges (close to andesitic compositions) (Castro et al., 2010), the first emplaced leucocratic granodiorites show trace element contents similar to the experimental results where the P-T conditions favoured the stability of Grt at the source, while the youngest group of Flamenco samples present REE patterns such as those in Grt-free experiments (Fig. 12a). Accounting for the Sr/Y vs. Y (Fig. 6f) and the Ce/Yb vs. Yb (Fig. 12b) relations, which are related to the presence of Grt in the solid residue at the magmatic source (Moyen, 2009; Castro et al., 2010), the SW granodiorites show lower Y and Yb contents and higher Sr/Y and Ce/Yb ratios. Therefore, these rocks are plotted in the Grt-present field according to the subduction mélange experiments, while the rest of the Flamenco tonalites and granodiorites are represented in the Grt-free area (Fig. 12b). These high Yb contents and the low Ce/Yb ratios described for the Lower Jurassic magmas of the Flamenco pluton are mostly coincident with representative Jurassic intrusives of the Coastal batholith (Parada et al., 1999; Coloma et al., 2017), as the two samples from the Montegrande granites, which yield Upper Triassic ages (Coloma et al., 2017), are plotted in the Grt-free and Grt-present areas (Fig. 12b).

At a given temperature, the stability field of Grt increases and the field of Pl decreases with pressure, determining the increase of Sr and LREE partitioning in the melt relative to Y and HREE respectively, fixed by a Grt-present solid assemblage (Moyen, 2009). Further, the phase relations in the mixed MORB-metasediments sources show that lower temperatures and, therefore, lower partial melting percentages favored the stability of Grt in the solid assemblage (Castro et al., 2010). The coincidence in the SW older leucocratic granodiorites of lower Yb contents (Fig. 12, Table 1), the absence of the Eu anomaly (Figs. 6 and 12), the high Sr contents (Fig. 6e) and the more silicic leucocratic characteristic point to a melt generated in presence of Grt + Px and minor Pl, which is characteristic of low melt fractions generated at temperatures below 1100 °C and/or pressures above >1.5 GPa (50–60 km) (Castro et al., 2010). For the Coastal Range batholith, this short-range geochemical evolution described in the Flamenco pluton may be achieved during the establishment of a stable magmatic source beneath the Andean arc. In the Upper Triassic, the renewal of the subduction process or the steepening of the slab, depending on the tectonic interpretation of the transition between the pre-Andean and Andean cycles (Mpodozis and Kay, 1992; Del Rey et al., 2016; Fuentes et al., 2017; Coloma et al., 2017), may involve a cold oceanic crust that reached deeper areas in the mantle before the first melts were generated under lower T and/or higher P conditions, hence more fractionated and more silicic (Gerya et al.,

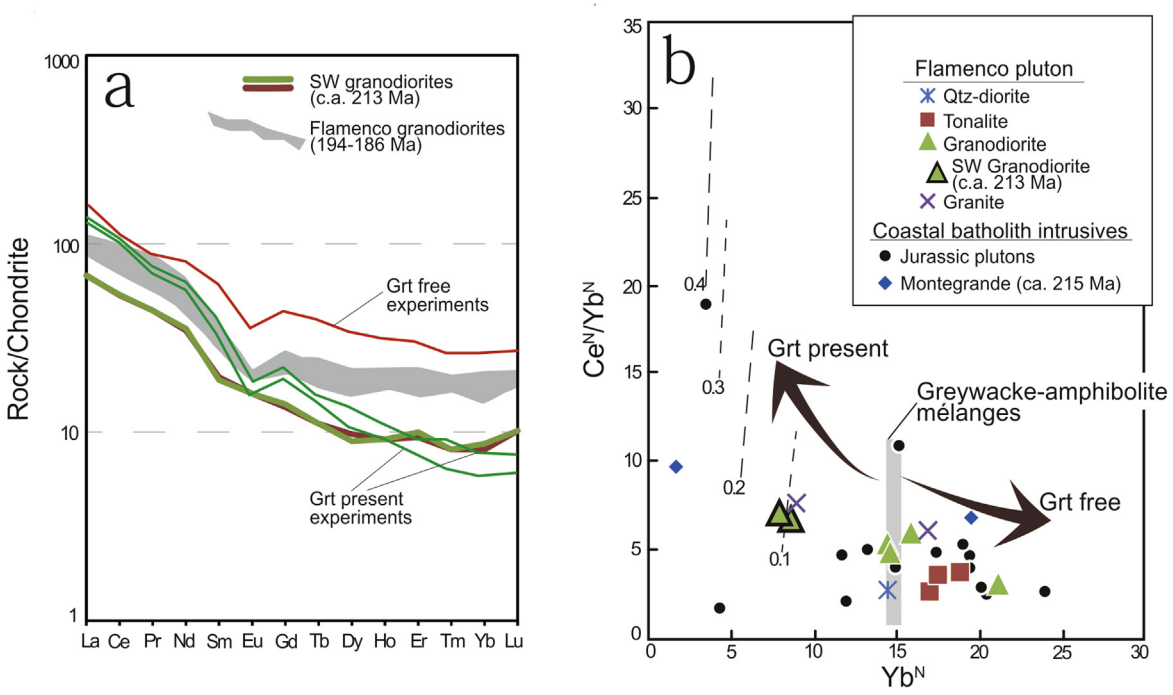

Figure 12. (a) Chondrite-normalized (Nakamura, 1974) REE diagram for the early SW leucocratic granodiorites (c.a. 213 Ma) and for the rest of the younger studied granodiorites (194-186 Ma) from the Flamenco pluton. REE patterns obtained for Grt-free and Grt-present experimental assemblages in subducted mélange (aprox. andesitic) compositions (Castro et al., 2010) are plotted for comparison. (b) Ce_N/Yb_N vs. Yb_N diagram showing the geochemical differences between the SW leucocratic granodiorites and the rest of the samples of the Flamenco pluton. Limarí and Papudo-Quintero Jurassic intrusive complexes (Parada et al., 1999) and Montegrande granites (Coloma et al., 2017) are plotted for comparison. The Grt-free and Grt-present fields are experimentally calculated for a greywacke-amphibolite mixed source (Castro et al., 2010) depicting the "adakitic" trends (high Ce_N/Yb_N and low Yb_N contents). Dashed lines represent the Grt wt.% in the experimental assemblages.

Please cite this article in press as: Rodríguez, N., et al., The significance of U–Pb zircon ages in zoned plutons– the case of the Flamenco pluton, Coastal Range batholith, northern Chile, Geoscience Frontiers (2018), https://doi.org/10.1016/j.gsf.2018.06.003

2004; Castro and Gerya, 2008). A deeper source area most likely associated with a thickened crust that was progressively stretched through the Jurassic magmatic evolution may also be considered (Kleiman and Japas, 2009; Echaurren et al., 2017; González et al., 2017). Subsequently, mostly from the Lower Jurassic, the subduction process attained a more stable organization, with shallower and/or hotter magmatic sources. This more mature tectonic setting originated a long-lasting, huge and homogeneous magmatic source that was active in the convergent margin during, at least, 100 Ma.

6.3. *The onset of the Cordilleran-type magmatism (Andean cycle) in the western margin of South America*

The inception of the Andean cycle has been traditionally proposed in the Lower Jurassic according to the age of the first intrusives emplaced in the magmatic arc and the volcanic rocks of the arc (La Negra Formation in northern Chile) (Berg and Breitkreuz, 1983; Godoy and Lara, 1998; Parada et al., 1999; Oliveros, 2005). New geochronological results yielded by the westernmost calc-alkaline Cordilleran-type granitoids of the Coastal Range batholith (this study; Coloma et al., 2017), suggest that the new paleogeographic configuration that located the magmatic arc 100 km to the west relative to its late Paleozoic location, started before 213 Ma (Upper Triassic). The geochronological characterization of the tectonic process that promoted such changes prior to the break-up of the Gondwana megacontinent during Triassic times depends on the hypothesis proposed for the pre-Andean events, including the accretion of terranes or oceanic island complexes to the margin (Mpodozis and Kay, 1992; Fuentes et al., 2017) and the steepening of the subduction angle (Coloma et al., 2017). The time lapse from the set up of a subductive margin to the generation of the first subduction-related magmatism should be considered too (Annen et al., 2006; Gerya and Stoeckhert, 2006; Gorczyk et al., 2007; Castro et al., 2010). In any case, the geochronological results presented in this work date the first Andean magmatism in Upper Triassic times rather than Lower Jurassic.

7. Conclusions

This study of the zoned Flamenco pluton presents evidences obtained from the field relations, geochemistry and U–Pb zircon geochronology of the magmatic facies that form the intrusive complex and allow us to propose an accurate description of the emplacement process. The recognition of different sets of co-genetic crystals (antecrysts, autocrysts) in a zircon sample leads to the interpretation of individual and group ages rather than other statistic, likely meaningless, ages. The interpretation of these groups of analyses selected to obtain the crystallization ages and the emplacement sequence of the Flamenco pluton was backed up with geochemical and field evidences.

The Flamenco pluton, part of the westernmost Late Triassic to Lower Cretaceous Andean magmatic arc in northern Chile, is composed of three distinguishable domains based on their geochemistry, crystallization ages and emplacement sequence. The SW domain of the pluton is constituted by mostly homogeneous leucocratic granodiorites that yielded an age of ca. 213 Ma as the best estimation for the emplacement age. This oldest intrusive unit shows the highest Sr, Sr/Y and Ce/Yb values among the granodioritic facies of the pluton. These data, together with the absence of the Eu anomaly and the depletion in HREE, point to the presence of Grt and minor Pl in the source area, and therefore lower T and/or higher P conditions, during this early stage of the magmatic arc building.

The northwest and east domains of the Flamenco pluton are composed of gabbros, Qtz-diorites, tonalites, granodiorites and granites with calcic, magnesian and metaluminous characteristics. The range of crystallization ages obtained for these magmatic facies, between 194 and 186 Ma, and the similar geochemical trends described by these samples point to a similar origin and emplacement process for these domains of the pluton. However, the detailed study of the geochronological results and the field relations depict interesting differences between both areas. To the northwest, the Flamenco pluton presents an obvious zonation between a mafic external area (Qtz-diorites and tonalites), including intrusive gabbroic bodies, and a granodioritic to granitic inner zone. Geochronological results show that the inner felsic magmas were emplaced at 192 ± 1.5 Ma, while the external Qtz-diorites yield two main age groups of 191.4 ± 1.9 Ma and 186.3 ± 1.8 Ma. The latter is interpreted as the best estimate for the crystallization age of the external mafic zone in the NW domain of the pluton. The granoblastic textures and the recrystallized zircons observed in the granodiorites (FL-16-12) located at the contact between the felsic inner and the mafic external zones are in agreement with a late emplacement of the Qtz-dioritic facies between the previously formed granodioritic-granitic inner area and the host metasediments. Although the E domain of the pluton is also characterized by the presence of gabbros and Qtz-diorites close to the contacts with the host-rocks, intrusive gabbroic tabular bodies show mingling evidences in the contact zone with the tonalites and granodiorites that comprise most of this domain. These field relations suggest the simultaneous coexistence of both felsic and mafic magmas at the emplacement level, which is in agreement with the geochronological results. Gabbros and granodiorites in the E domain present an older age group that yields 194.7–193.1 Ma and a younger group with ages of 188.3 ± 2.1 Ma and 185.5 ± 1.4 Ma for the gabbros and the granodiorites respectively. The slight age differences found in these younger groups may be related to the faster crystallization process in the gabbroic magmas that finally register sub-solidus fabrics. The observed differences in the emplacement processes between these geochemically similar domains may be related to the variations in the magmatic addition rates, which promoted the more extended preservation of the super-solidus conditions in the E domain, as is supported by the wider age ranges yielded by these eastern facies.

The normal zonation described by the Lower Jurassic intrusive units of the Flamenco pluton is determined by the latter emplacement of the mafic external facies, and is not related to in-situ differentiation processes between these magmas. An increase in the mafic component in the intrusive magmas is coincident with the evolution of the Th/U ratios in the analyzed zircons, which are considerably higher (0.84 vs. 0.68) for zircons with ages younger than 190 Ma. Nevertheless, the genetic relation between older and younger intrusive units of the Flamenco pluton is confirmed by the presence of antecrysts in most of the studied samples that give similar ages around 200 Ma, 213 Ma and 220 Ma. The inclusion of these co-genetic older zircon crystals in the new magma batches may be produced in the source area or by remobilization of previously intruded crystal mushes. Finally, the presence in the zircons analyzed in the host metasediments of metamorphic overgrowths with similar ages (228 Ma and 204 ± 5 Ma) suggests that the inception of the Cordilleran-type magma source and magmatic arc in the Andean cycle go back to Upper Triassic times in northern Chile.

Acknowledgments

This work is part of the PhD studies of Natalia Rodríguez, carried out at the Department of Geology of the University of Atacama (Chile) and the University of Freiberg (Germany). The study has been funded with FONDECYT Project No. 11140722 of CONICYT, and

with the fund support of DIUDA 2013-22268 and DIUDA 2014-22273 projects. We would like to sincerely thank the editor and the reviewers of Geoscience Frontiers for their thorough corrections of the first draft of this manuscript. We would also like to express our gratitude to the staff of the Geochronological Research Center of the University of São Paulo for their kindness and facility.

Appendix A. Supplementary data

Supplementary data related to this article can be found at https://doi.org/10.1016/j.gsf.2018.06.003.

References

Alonso Perez, R., Müntener, O., Ulmer, P., 2009. Igneous garnet and amphibolite fractionation in the roots of island arcs: experimental constraints on andesite liquids. Contributions to Mineralogy and Petrology 157, 541–558.

Annen, C., Blundy, J.D., Sparks, R.S.J., 2006. The genesis of intermediate and silicic magmas in deep crustal hot zones. Journal of Petrology 47, 505–539.

Arabasz, W.J., 1971. Geological and Geophysical Studies of the Atacama Fault Zone in Northern Chile. PhD thesis. Californian Institute of Technology, Pasadena.

Aragón, E., Castro, A., Díaz-Alvarado, J., Pinotti, L., D'eramo, F., Demartis, M., Coniglio, J., Hernando, I., Rodríguez, C., 2017. Mantle derived crystal-poor rhyolitic ignimbrites: eruptive mechanism from geochemical and geochronological data of the Piedra Parada caldera, Southern Argentina. Geoscience Frontiers. https://doi.org/10.1016/j.gsf.2017.09.004.

Arévalo, C., Welkner, D., 2008. Geología del área Carrizal Bajo-Chacritas, Región de Atacama. In: Servicio Nacional de Geología y Minería, Carta Geológica de Chile, Serie Geología Básica, vol. 111, p. 67, 1 mapa 1:100.000.

Bachmann, O., Dungan, M.A., Lipman, P.W., 2002. The Fish Canyon magma body, San Juan volcanic field, Colorado; rejuvenation and eruption of an upper-crustal batholith. Journal of Petrology 43, 1469–1503.

Bachmann, O., Bergantz, G.W., 2004. On the origin of crystal-poor rhyolites: extracted from batholithic crystal mushes. Journal of Petrology 45, 1565–1582.

Bachmann, O., Bergantz, G.W., 2008. The magma reservoirs that feed super-eruptions. Elements 4, 19–23.

Bachmann, O., Huber, C., 2016. Silicic magma reservoirs in the Earth's crust. American Mineralogist 101, 2377–2404.

Bea, F., Montero, P., 2013. Diffusion-induced disturbances of the U–Pb isotope system in pre-magmatic zircon and their influence on SIMS dating. A numerical study. Chemical Geology 349–350, 1–17.

Bell, C.M., 1982. The lower paleozoic metasedimentary basament of the coastal ranges of Chile between 25°30' and 27°S. Revista Geologica de Chile 17, 21–29.

Bell, C.M., 1987. The origin of the upper Palaeozoic Chanaral mélange of N Chile. Journal of the Geological Society London 144, 599–610.

Berg, K., Breitkreuz, C., 1983. Mesozoische Plutone in der nordchilenischen Küstenkordillere: Petrogenese, Geochronologie, Geochemie und Geodynamik mentelbetonter Magmatite. Geotektonische Forschungen 66, 107.

Black, L.P., Jagodzinski, E.A., 2003. Importance of establishing sources of uncertainty for the derivation of reliable SHRIMP ages. Australian Journal of Earth Sciences 50, 503–512.

Bouchez, J.L., 1997. Granite is never isotropic: an introduction to AMS studies of granitc rocks. In: Bouchez, J.L., Hutton, D.H.W., Stephens, W.E. (Eds.), Granite: From Segregation of Melt to Emplacement Fabrics. Kluwer, Dordrecht, pp. 95–112.

Brown, M., Díaz, F., Grocott, J., 1993. Displacement history and tectonic significance of the El Salado segment of the Atacama Fault System, Northern Chile. GSA Bulletin 105, 1165–1174.

Burgisser, A., Bergantz, C.W., 2011. A rapid mechanism to remobilize and homogenize highly crystalline magma bodies. Nature 471, 212–215.

Cao, W., Paterson, S., Saleeby, J., Zalunardo, S., 2016. Bulk arc strain, crustal thickening, magma emplacement, and mass balances in the Mesozoic Sierra Nevada arc. Journal of Structural Geology 84, 14–30.

Castro, A., 2013. Tonalite-granodiorite suites as cotectic systems: a review of experimental studies with application to granitoid petrogenesis. Earth-science Reviews 124, 68–95.

Castro, A., Gerya, T.V., 2008. Magmatic implications of mantle wedge plumes: Experimental study. Lithos 103, 138–148.

Castro, A., Gerya, T., García-Casco, A., Fernández, C., DíazAlvarado, J., Moreno-Ventas, I., Loew, I., 2010. Melting relations of MORB-sediment mélanges in underplated mantle wedge plumes. Implications for the origin of cordilleran-type batholiths. Journal of Petrology 51, 1267–1295.

Castro, A., Moreno-Ventas, I., Fernández, C., Vujovich, G., Gallastegui, G., Heredia, N., Martino, R.D., Becchio, R., Corretgé, L.G., Díaz-Alvarado, J., García-Arias, M., Liu, D.-Y., 2011. Petrology and SHRIMP U-Pb zircon geochronology of Cordilleran granitoids of the Bariloche area, Argentina. Journal of South American Earth Sciences 32, 508–530.

Castro, A., Díaz-Alvarado, J., Fernández, C., 2014. Fractionation and incipient self-granulitization during deep-crust emplacement of Lower Ordovician Valle Féritl batholith at the Gondwana active margin of South America. Gondwana Research 25, 685–706.

Chamberlain, K.J., Wilson, C.J.N., Wooden, J.L., Charlier, B.L.A., Ireland, T.R., 2014. New perspectives on the Bishop tuff from zircon textures, ages and trace elements. Journal of Petrology 55, 395–426.

Chapman, J.B., Ducea, M.N., Profeta, L., DeCelles, P.G., 2015. Tracking changes in crustal thickness during orogenic evolution with Sr/Y; an example from the Western U.S. Cordillera. Geology 43, 919–923.

Charlier, B.L.A., Wilson, C.J.N., Lowenstern, J.B., Blake, S., van Calsteren, P.W., Davidson, J.P., 2005. Magma generation at a large, hyperactive silicic volcano (Taupo, New Zealand) revealed by U–Th and U–Pb systematics in zircons. Journal of Petrology 46, 3–32.

Charrier, R., Pinto, L., Rodríguez, M.P., 2007. Tectonostratigraphic evolution of the Andean orogen in Chile. In: Moreno, T., Gibbons, W. (Eds.), The Geology of Chile, the Geological Society, Londres, pp. 21–114.

Chen, L., Zhao, Z., 2017. Origin of continental arc andesites: The composition of source rocks is the key. Journal of Asian Earth Sciences 145, 217–232.

Cherniak, D.J., 2010. Diffusion in accessory minerals: zircon, titanite, apatite, monazite and xenotime. Reviews in Mineralogy and Geochemistry 72, 827–869.

Chiaradia, M., 2015. Crustal thickness control on Sr/Y signatures of recent arc magmas: an Earth scale perspective. Scientific Reports 5, 8115. https://doi.org/10.1038/srep08115.

Clemens, J.D., Stevens, G., Farina, F., 2011. The enigmatic sources of I-type granites: the peritectic connexion. Lithos 126 (3–4), 174–181.

Clemens, J.D., Stevens, G., 2012. What controls chemical variation in granitic magmas? Lithos 134–135, 317–329.

Coleman, D.S., Gray, W., Glazner, A.F., 2004. Rethinking the emplacement and evolution of zoned plutons: geochronologic evidence for incremental assembly of the Tuolumne Intrusive Suite, California. Geology 32, 433–436.

Coloma, F., Valin, X., Oliveros, V., Vásquez, P., Creixell, C., Salazar, E., Ducea, M.N., 2017. Geochemistry of Permian to Triassic igneous rocks from northern Chile (28o-30o15'S): Implications on the dynamics of the proto-Andean margin. Andean Geology 44 (2), 147–178.

Compston, W., 2001. Effect of Pb loss on the ages of reference zircons QGNG and SL 13, and of volcanic zircons from the Early Devonian Merrions and Turondale Formations, New South Wales. Australian Journal of Earth Sciences 48, 797–803.

Cooper, K.M., Kent, A.J.R., 2014. Rapid remobilization of magmatic crystals kept in cold storage. Nature 506, 480–483.

Corfu, F., Hanchar, J.M., Hoskin, P.W.O., Kinny, P., 2003. Atlas of zircon textures. In: Hanchar, J.M., Hoskin, P.W.O. (Eds.), Zircon. Reviews in Mineralogy and Geochemistry, vol. 53. Mineralogical Society of America, Washington DC, pp. 27–62.

Creixell, C., Ortiz, M., Arévalo, C., 2012. Geología del área Carrizalillo-El Tofo, Regiones de Atacama y Coquimbo. In: Servicio Nacional de Geología y Minería, Carta Geológica de Chile, Serie Geología Básica, 133–134, p. 82, 1 mapa 1:100.000.

Cummings, G.L., Richards, J.R., 1975. Ore lead isotope ratios in a continuously changing Earth. Earth and Planetary Science Letters 28, 155–171.

Dallmeyer, R.D., Brown, M., Grocott, J., Taylor, G.K., Treloar, P.J., 1996. Mesozoic magmatic and tectonics events within the Andean Plate boundary zone, 26o-27o30'S, North Chile: constraints from $^{40}Ar/^{39}Ar$ Mineral ages. The Journal of Geology 104 (1), 19–40.

De La Roche, H., Leterrier, J., Grandclaude, P., Marchal, M., 1980. A classification of volcanic and plutonic rocks using R1R2-diagram and major element analyses. Its relationships with current nomenclature. Chemical Geology 29, 183–210.

De Paolo, D.J., 1981. A neodymiun and strontium isotopic study of the Mesozoic calc-alkaline granitic batholiths of the Sierra Nevada and Peninsular Ranges, California. Journal of Geophysical Research 86, 10470–10488.

de Saint Blanquat, M., Horsman, E., Habert, G., Morgan, S., Vanderhaeghe, O., Law, R., Tikoff, B., 2011. Multiscale magmatic cyclicity, duration of pluton construction, and the paradoxical relationship between tectonism and plutonism in continental arcs. Tectonophysics 500, 20–33.

Del Rey, A., Arriagada, C., Dekart, K., Martínez, F., 2016. Resolving the paradigm of the late Paleozoic-Triassic Chilean magmatism: Isotopic approach. Gondwana Research 37, 172–181.

DeCelles, P.G., Ducea, M.N., Kapp, P., Zandt, G., 2009. Cyclicity in Cordilleran orogenic systems. Nature Geoscience 2, 251–257.

Díaz-Alvarado, J., 2017. Experimental early crystallization of K-feldspar in granitic systems. Implications on the origin of magmatic fabrics in granitic rocks. Geológica Acta. https://doi.org/10.1344/%25x.

Díaz-Alvarado, J., Castro, A., Fernández, C., Moreno-Ventas, I., 2011. Assessing bulk assimilation in cordierite-bearing granitoids from the Central System batholith, Spain; experimental, geochemical and geochronological constraints. Journal of Petrology 52, 223–256.

Díaz-Alvarado, J., Fernández, C., Díaz Azpiroz, M., Castro, A., Moreno-Ventas, I., 2012. Fabric evidence for granodiorite emplacement with extensional shear zones in the Variscan Gredos massif (Spanish Central System). Journal of Structural Geology 42, 74–90.

Díaz-Alvarado, J., Fernández, C., Castro, A., Moreno-Ventas, I., 2013. SHRIMP U–Pb zircon geochronology and thermalmodeling of multilayer granitoid intrusions. Implications for the building and thermal evolution of the Central System batholith, Iberian Massif, Spain. Lithos 175–176, 104–123.

Ducea, M.N., Bergantz, G., Saleeby, J.B., 2015a. The architecture, chemistry and evolution of continental magmatic arcs. Annual Review of Earth and Planetary Sciences 43, 299–331.

Ducea, M.N., Paterson, S.R., DeCelles, P.G., 2015b. High-volume magmatic events in subduction systems. Elements 11, 99–104.
Echaurren, A., Oliveros, V., Folguera, A., Ibarra, F., Creixell, C., Lucassen, F., 2017. Early Andean tectonomagmatic stages in north Patagonia: insights from field and geochemical data. Journal of the Geological Society 174 (3), 405–421.
Fiannacca, P., Cirrincione, R., Bonanno, F., Carciotto, M.M., 2015. Source-inherited compositional diversity in granite batholiths: the geochemical message of Late Paleozoic intrusive magmatism in central Calabria (southern Italy). Lithos 236–237, 123–140.
Fiannacca, P., Williams, I.S., Cirrincione, R., 2017. Timescales and mechanisms of batholith construction: Constraints from zircon oxygen isotopes and geochronology of the late Variscan Serre Batholith (Calabria, southern Italy). Lithos 277, 302–314.
Frost, B.R., Barnes, C.G., Collins, W.J., Arculus, R.J., Ellis, D.J., Frost, C.D., 2001. A geochemical classification for granitic rocks. Journal of Petrology 42, 2033–2048.
Frost, C.D., Frost, B.R., Beard, J.S., 2016. On silica-rich granitoids and their eruptive equivalents. American Mineralogist 101, 1268–1284.
Fuentes, P., Díaz-Alvarado, J., Fernández, C., Díaz-Azpiroz, M., Rodríguez, N., 2016. Structural analysis and shape-preferred orientation determination of the mélange facies in the Chañaral mélange, Las Tórtolas Formation, Coastal Cordillera, northern Chile. Journal of South American Earth Sciences 67, 40–56.
Fuentes, P., Díaz-Alvarado, J., Rodríguez, N., Fernandez, C., Breitkreuz, C., Contreras, A., 2017. Geochemistry, petrogenesis and tectonic significance of the volcanic rocks of the Las Tortolas Formation, Coastal Cordillera, northern Chile. Journal of South American Earth Sciences. https://doi.org/10.1016/j.jsames.2017.11.006.
Gana, P., Tosdal, R.M., 1996. Geocronología U–Pb y K–Ar en intrusivos del Paleozoico y Mesozoico de la Cordillera de la Costa, región de Valparaíso, Chile. Revista Geologica de Chile 23, 151–164.
Gerya, T.V., Yuen, D.A., Sevre, E.O.D., 2004. Dynamical causes for incipient magma chambers above slabs. Geology 32, 89–92.
Gerya, T.V., Stoeckhert, B., 2006. 2-D numerical modeling of tectonic and metamorphic histories at active continental margins. International Journal of Earth Sciences 95, 250–274.
Glazner, A.F., Bartley, J.M., Coleman, D.S., Gray, W., Taylor, R.Z., 2004. Are plutons assembled over millions of years by amalgamation from small magma chambers. Geological Society of America Today 14, 4–11.
Godoy, E., Lara, L., 1998. Hojas Chañaral y Diego de Almagro. Servicio Nacional de Geología y Minería. Mapas Geológicos, pp. 5–6 (1:100.000), Santiago.
González, J., Oliveros, V., Creixell, C., Velásquez, R., Vásquez, P., Lucassen, F., 2017. The Triassic magmatism and its relation with the Pre-Andean tectonic evolution: Geochemical and petrographic constrains from the High Andes of north central Chile (29º30' - 30ºS). Journal of South American Earth Sciences. https://doi.org/10.1016/j.jsames.2017.12.009.
Gorczyk, W., Gerya, T.V., Connolly, J.A.D., Yuen, D.A., 2007. Growth and mixing dynamics of mantle wedge plumes. Geology 35, 587–590.
Grocott, J., Taylor, G.K., 2002. Magmatic arc fault systems, deformation partitioning and emplacement of granitic complexes en the Coastal Cordillera, north Chilean Andes (25º30'S to 27º30'S). Journal of the Geological Society London 159, 425–442.
Grove, T.L., Baker, M.B., Price, R.C., Parman, S.W., Elkins-Tanton, L.T., Chatterjee, N., Muntener, O., 2005. Magnesian andesite and dacite lavas from Mt. Shasta, northern California: Products of fractional crystallization of H_2O-rich mantle melts. Contributions to Mineralogy and Petrology 148, 542–565.
Hawkesworth, C.J., Kemp, A.I.S., 2006. Evolution of the continental crust. Nature 443, 811–817.
Hecht, L., Vigneresse, J.L., Morteani, J., 1997. The origin of compositional zoning of the Fichtelgebirge pluton (Germany): Evidence from a gravimetric and geochemical study. Geologische Rundschau 86, 93–109.
Hecht, L., Vigneresse, J.L., 1999. A multidisciplinary approach combining geochemical, gravity and structural data: implications for pluton emplacement and zonation. In: Castro, A., Fernández, C., Vigneresse, J.L. (Eds.), Understanding Granites: Integrating New and Classical Techniques, vol. 168. Geological Society of London Special Publication, pp. 95–110.
Hervé, F., Pankhurst, R.J., Fanning, C.M., Calderon, M., Yaxley, G.M., 2007. The South Patagonian batholith: 150 my of granite magmatism on a plate margin. Lithos 97, 373–394.
Hildreth, W., Moorbath, S., 1988. Crustal contributions to arc magmatism in the Andes of central Chile. Contributions to Mineralogy and Petrology 98, 455–489.
Huber, C., Bachmann, O., Manga, M., 2010. Two competing effects of volatiles on heat transfer in crystal-rich magmas: thermal insulation vs. defrosting. Journal of Petrology 51, 847–867.
Huber, C., Bachmann, O., Dufek, J., 2011. Thermo-mechanical reactivation of locked crystal mushes: Melting-induced internal fracturing and assimilation processes in magmas. Earth and Planetary Science Letters 304, 443–454.
Iriarte, S., Arévalo, C., Mpodozis, C., 1999. Hoja La Guardia, Región de Atacama. Servicio Nacional de Geología y Minería (Chile). Mapas Geológicos Nº13, 1 mapa escala 1:100.000, Santiago.
Jeon, H., Williams, I.S., Chappell, B.W., 2012. Magma to mud to magma: rapid crustal recycling by Permian granite magmatism near the eastern Gondwana margin. Earth and Planetary Science Letters 319–320, 104–117.
Jeon, H., Whitehouse, M.J., 2014. A critical evaluation of u–pb calibration schemes used in SIMS zircon geochronology. Geostandards and Geoanalytical Research 39, 443–452.
Kelemen, P.B., Hanghoj, K., Greene, A.R., 2003. One view of the geochemistry of subduction-related magmatic arcs, with emphasis on primitive andesite and lower crust. In: Rudnick, R.L. (Ed.), The Crust. Elsevier, Amsterdam, pp. 593–659.
Kirsch, M., Paterson, S.R., Wobbe, F., Martínez Ardila, A.M., Clausen, B.L., Alasino, P.H., 2016. Temporal histories of Cordilleran continental arcs: testing models for magmatic episodicity. American Mineralogist 101, 2133–2154.
Kleiman, L.E., Japas, M.S., 2009. The Choiyoi volcanic province at 34°S–36°S (San Rafael, Mendoza, Argentina): Implications for the Late Palaeozoic evolution of the southwestern margin of Gondwana. Tectonophysics 473 (3–4), 283–299.
Kretz, R., 1983. Symbols for rock-forming minerals. American Mineralogist 68, 277–279.
Le Bas, M.J., Le Maitre, R.W., Streckeisen, A., Zanettin, B., 1986. A chemical classification of volcanic rocks based on the total alkali-silica diagram. Journal of Petrology 27, 745–750.
Ludwig, K.J., 2003. Isoplot 3.00. Berkeley Geochronology Center Special Publication, 4, 70pp.
Maksaev, V., Munizaga, F., Tassinari, C., 2014. Timing of the magmatism of the paleo-Pacific border of Gondwana: U-Pb geochronology of Late Paleozoic to Early Mesozoic igneous rocks of the north Chilean Andes between 20° and 31°S. Andean Geology 41, 447–506.
McKay, M.P., Weislogel, A.L., Fildani, A., Brunt, R.L., Hodgson, D.M., Flint, S.S., 2015. U-PB zircon tuff geochronology from the Karoo Basin, South Africa: implications of zircon recycling on stratigraphic age controls. International Geology Review 57, 393–410.
Miller, C., Wooden, J., 1994. Anatexis, hybridization, and the modification of ancient crust: mesozoic plutonism in the Old Woman Mountains area, California. Lithos 32, 111–133.
Miller, C.F., McDowell, S.M., Mapes, R.W., 2003. Hot and cold granites? Implications of zircon saturation temperatures and preservation of inheritance. Geology 31, 529–532.
Miller, J.S., Matzel, J.E.P., Miller, C.F., Burgess, S.D., Miller, R.B., 2007. Zircon growth and recycling during the assembly of large, composite arc plutons. Journal of Volcanology and Geothermal Research 167, 281–299.
Miller, C.F., Furbish, D.J., Walker, B.A., Claiborne, L.L., Koteas, G.C., Bleick, H.A., Miller, J.S., 2011. Growth of plutons by incremental emplacement of sheets in crystal-rich host: Evidence from Miocene intrusions of the Colorado River region, Nevada, USA. Tectonophysics 500, 65–77.
McKay, M.P., Jackson Jr., W.T., Hessler, A.M., 2018. Tectonic stress regime recorded by zircon Th/U. Gondwana Research 57, 1–9.
Moyen, J.F., 2009. High Sr/Y and La/Yb ratios: the meaning of the "adakitic signature". Lithos 112, 556–574.
Mpodozis, C., Kay, S., 1992. Late Paleozoic to Triassic evolution of the pacific Gondwana margin: evidence from Chilean frontal Cordilleran batholiths. The Geological Society of America Bulletin 104, 999–1014.
Mpodozis, C., Ramos, V.A., 1989. The Andes of chile and argentina. In: Ericksen, G.E., Cañas Pinochet, M.T., Reinemud, J.A. (Eds.), Geology of the Andes and its Relation to Hydrocarbon and Mineral Resources: Circumpacific Council for Energy and Mineral Resources, Earth Sciences Series, vol. 11, pp. 59–90.
Nakamura, N., 1974. Determination of REE, Ba, Fe, Mg, Na and K in carbonaceous and ordinary chondrites. Geochimica et Cosmochimica Acta 38, 757–775.
Oliveros, V., 2005. Étude geochronologique des unités jurassiques et Crétacé Inférieur du Noprd du Chili (18º30'-24ºS, 60º30'-70º30'W): Origine, mise en place, altération, métamorphisme et minéralisations associées. Thesis. Université de Nice-Sophia Antipolis and Depatamento de Geología, Universidad de Chile, Santiago.
Otamendi, J.E., Vujovich, G.I., De la Rosa, J.D., Tibaldi, A.M., Castro, A., Martino, R.D., Pinotti, L.P., 2009. Geology and petrology of a deep crustal zone from the Famatinian paleo-arc, Sierras de Valle Fértil and La Huerta, San Juan, Argentina. Journal of South American Earth Sciences 27, 258–279.
Pankhurst, R.J., Weaver, S.D., Hervé, F., Larrondo, P., 1999. Mesozoic-Cenozoic evolution of the North Patagonian Batholith in Aysen, southern Chile. Journal of the Geological Society 156, 673–694.
Pappalardo, L., Mastrolorenzo, G., 2012. Rapid differentiation in a sill-like magma reservoir: a case study from the Campi Flegrei caldera. Scientific Reports 2.
Parada, M.A., 1992. Contribución a la geoquímica del complejo Plutónico Papudo-Quinteros, Chile central: implicancias petrogenéticas. Revista Geologica de Chile 19, 199–210.
Parada, M.A., Nyström, J.O., Levi, B., 1999. Multiple sources for the coastal batholith of central Chile (31-34ºS): Geochemical and Sr-Nd isotopic evidence and tectonic implications. Lithos 46, 505–521.
Parada, M.A., López-Escobar, L., Oliveros, V., Fuentes, F., Morata, D., Calderón, M., Aguirre, L., Féraud, G., Espinoza, F., Moreno, H., Figueroa, O., Muñoz Bravo, J., Troncoso Vásquez, R., Stern, C.R., 2007. Andean Magmatism. In: Moreno, T., Gibbons, W. (Eds.), The Geology of Chile, the Geological Society, Londres, pp. 115–146.
Paterson, S.R., Zák, J., Janouzek, V., 2008. Growth of complex sheeted zones during recycling of older magmatic units into younger: Sawmill Canyon area, Tuolumne batholith, Sierra Nevada, California. Journal of Volcanology and Geothermal Research 177, 457–484.
Paterson, S.R., Okaya, D., Memeti, V., Economos, R., Miller, R.B., 2011. Magma addition and flux calculations of incrementally constructed magma chambers in continental margin arcs: Combined field, geochronologic, and thermal modeling studies. Geosphere 7, 1439–1468.
Paterson, S.R., Ducea, M.N., 2015. Arc magmatic tempos: gathering the evidence. Elements 11, 91–98.

Please cite this article in press as: Rodríguez, N., et al., The significance of U–Pb zircon ages in zoned plutons– the case of the Flamenco pluton, Coastal Range batholith, northern Chile, Geoscience Frontiers (2018), https://doi.org/10.1016/j.gsf.2018.06.003

Patiño-Douce, A.E., 1995. Experimental generation of hybrid silicic melts by reaction of high-Al basalt with metamorphic rocks. Journal of Geophysical Research 100, 15623–15639.

Pearce, J.A., Harris, N.B.W., Tindle, A.G., 1984. Trace element discrimination diagrams forthe tectonic interpretation of granitic rocks. Journal of Petrology 25, 956–983.

Pereira, M.F., Chichorro, M., Johnston, S.T., Gutierrez-Alonso, G., Silva, J.B., Linnemann, U., Hofmann, M., Drost, K., 2012. The missing Rheic Ocean magmatic arcs: provenance analysis of Late Paleozoic sedimentary clastic rocks of SW Iberia. Gondwana Research 22, 882–891.

Pereira, M.F., Castro, A., Chichorro, M., Fernández, C., Díaz-Alvarado, J., Martí, J., Rodríguez, C., 2014. Chronological link between deep-seated processes in magma chambers and eruptions: Permo-Carboniferous magmatism in the core of Pangaea (Southern Pyrenees). Gondwana Research 25, 290–308.

Pereira, M.F., Chichorro, M., Moita, P., Santos, J.F., Solá, A.M.R., Williams, I.S., Silva, J.B., Armstrong, R.A., 2015. The multistage crystallization of zircon in calc-alkaline granitoids: U–Pb age constraints on the timing of Variscan tectonic activity in SW Iberia. International Journal of Earth Sciences 104, 1167–1183.

Petford, N., Cruden, A.R., McCaffrey, K.J.W., Vigneresse, J.L., 2000. Granite magma formation, transport and emplacement in the Earth's crust. Nature 408, 669–673.

Rapela, C.W., Tosseli, A., Heaman, L., Saavedra, J., 1990. Granite plutonism of the Sierras Pampeanas; an inner cordilleran Paleozoic arc in the southern Andes. In: Kay, S.M., Rapela, C.W. (Eds.), Plutonism from Antarctica to Alaska, Special Paper, vol. 241, pp. 77–90.

Rodríguez, N., Díaz-Alvarado, J., Rodríguez, C., Riveros, K., Fuentes, P., 2016. Petrology, geochemistry and thermobarometry of the northern area of the Flamenco pluton, Coastal Range batholith, northern Chile. A thermal approach to the emplacement processes in the Jurassic andean batholiths. Journal of South American Earth Sciences 67, 122–139.

Rubatto, D., 2002. Zircon trace element geochemistry: partitioning with garnet and the link between U–Pb ages and metamorphism. Chemical Geology 184, 123–138.

Rudnick, R.L., 1995. Making continental crust. Nature 378, 571–578.

Sato, K., Tassinari, C.C.G., Basei, M.A.S., Siga Júnior, O., Takashi, A.O., Souza, M.A., 2014. Sensitive High Resolution Ion Microprobe (SHRIMP IIe/MC) of the Institute of Geosciences of the University of São Paulo, Brazil: analytical method and first results. Revista do Instituto de Geociências – USP, Geol. USP, Sér. cient., São Paulo 14 (3), 18.

Scheuber, E., Bogdanic, T., Jensen, A., Reutter, K.J., 1994. Tectonic development of the North Chilean Andes in relation to plate convergence and magmatism since the Jurassic. In: Reutter, K.-J., Scheuber, E., Wigger, P. (Eds.), Tectonics of the Southern Central Andes. Structure and Evolution of an Active Continental Margin. Springer, Heidelberg, pp. 121–140.

Scheuber, E., González, G., 1999. Tectonics of the Jurassic-Early Cretaceous magmatic arc of the north Chilean Coastal Cordillera (22°-26°S): A story of crustal deformation along a convergent plate boundary. Tectonics 18, 895–910.

Sisson, T.W., Ratajeski, K., Hankins, W.B., Glazner, A.F., 2005. Voluminous granitic magmas from common basaltic sources. Contributions to Mineralogy and Petrology 148, 635–661.

Spencer, C.J., Kirkland, C.L., Taylor, R.J.M., 2016. Strategies towards statistically robust interpretations of in situ U-Pb zircon geochronology. Geoscience Frontiers 7, 581–589.

Steiger, R., Jaeger, E., 1977. Subcommission on geochronology: convention on the use of decay constants in geo- and cosmochronology. Earth and Planetary Science Letters 36, 359–362.

Suárez, M., Naranjo, J.A., Puig, A., 1985. Estratigrafía de la Cordillera de la Costa al sur de Taltal, Chile: Etapas iniciales de la evolución andina. Revista Geologica de Chile 24, 19–28.

Suárez, M., Bell, M., 1992. Triassic rift-related sedimentary basins in northern Chile (24°–29°S). Journal of South American Earth Sciences 6, 109–121.

Teixeira, R.J.S., Neiva, A.M.R., Silva, P.B., Gomes, M.E.P., Andersen, T., Ramos, J.M.F., 2011. Combined U-Pb geochronology and Lu–Hf isotope systematics by LAM–ICPMS of zircons from granites and metasedimentary rocks of Carrazeda de Ansiães and Sabugal areas, Portugal, to constrain granite sources. Lithos 125, 321–334.

Thompson, A.B., Matile, L., Ulmer, P., 2002. Some thermal constraints on crustal assimilation during fractionation of hydrous, mantle-derived magmas with examples from Central Alpine Batholiths. Journal of Petrology 43, 403–422.

Vigneresse, J.L., 1995. Control of granite emplacement by regional deformation. Tectonophysics 249, 173–186.

Vigneresse, J.L., Barbey, P., Cuney, M., 1996. Rheological transitions during partial melting and crystallization with application to felsic magma segregation and transfer. Journal of Petrology 37, 1579–1600.

Villaseca, C., Orejana, D., Belousova, E.A., 2012. Recycled metaigneous crustal sources for S- and I-type Variscan granitoids from the Spanish Central System batholith: constraints from Hf isotope zircon composition. Lithos 153, 84–93.

Wagner, L.S., Beck, S., Zandt, G., 2005. Upper mantle structure in the south central Chile subduction zone (30 to 36°S) 2005. Journal of Geophysical Research 110, B01308. https://doi.org/10.1029/2004JB003238.

Walker, B.A., Bergantz, G.W., Otamendi, J.E., Ducea, M.N., Cristofolini, E.B., 2015.

Wang, X., Griffin, W.L., Chen, J., Huang, P., Li, X., 2011. U and Th contents and Th/U ratios of zircon in felsic and mafic magmatic rocks: Improved zircon-melt distribution coefficients. Acta Geologica Sinica 85, 164–174.

Watson, E.B., Harrison, T.M., 1983. Zircon saturation revisited-temperature and composition effects in a variety of crustal magma types. Earth and Planetary Science Letters 64, 295–304.

Welkner, D., Arévalo, C., Godoy, E., 2006. Geología del área Freirina-El Morado, Región de Atacama. Servicio Nacional de Geología y Minería, Carta Geológica de Chile, Serie Geología Básica 100, p. 50, 1 mapa 1:100.000.

Wendt, I., Carl, C., 1991. The statistical distribution of the mean squared weighted deviation. Chemical Geology: Isotope Geoscience section 86, 275–285.

Williams, I.S., 1998. U-Th-Pb geochronology by ion microprobe. In: McKibben, M.A., Shanks, W.C., Ridley, W.I. (Eds.), Applications of Microanalytical Techniques to Understanding Mineralizing Processes. Reviews in Economic Geology, vol. 7, pp. 1–35.

Williams, I.S., 2001. Response of detrital zircon and monazite, and their U–Pb isotopic systems, to regional metamorphism and host-rock partial melting, Cooma Complex, southeastern Australia. Australian Journal of Earth Sciences 48, 557–580.

Wilson, M., 1989. Igneous Petrogenesis. A Global Tectonic Approach. Unwin Hyman, London, p. 466.

Wyllie, P.J., Huang, W.L., Stern, C.R., Maaloe, S., 1976. Granitic magmas: possible and impossible sources, water contents, and crystallization sequences. Canadian Journal of Earth Sciences 13, 1007–1019.

Wyllie, P.J., 1977. From Crucibles through Subduction to Batholiths. In: Saxena, S.K., Bhattacharjia (Eds.), Energetics of Geological Processes. Springer Verlag, pp. 389–433.

Please cite this article in press as: Rodríguez, N., et al., The significance of U–Pb zircon ages in zoned plutons– the case of the Flamenco pluton, Coastal Range batholith, northern Chile, Geoscience Frontiers (2018), https://doi.org/10.1016/j.gsf.2018.06.003